High energy behavior of $\gamma\gamma \to f\bar{f}$ processes in the standard model and minimal supersymmetric standard model

J. Layssac and F. M. Renard
Physique Mathématique et Théorique, UMR 5825, Université Montpellier II, F-34095 Montpellier Cedex 5, France
(Received 20 April 2001; published 13 August 2001)

We compute the leading logarithm electroweak contributions to $\gamma\gamma \to f\bar{f}$ processes in the standard model and minimal supersymmetric standard model. Several interesting properties are pointed out, such as the importance of the angular dependent terms, of the Yukawa terms, and especially of the $\tan^2\beta$ dependence in the supersymmetry contributions. These properties are complementary to those found in $e^+e^- \to f\bar{f}$. These radiative correction effects should be largely observable at future high energy $\gamma\gamma$ colliders. Polarized beams would give interesting checks of the structure of the one-loop corrections. We finally discuss the need for two-loop calculations and resummation.

DOI: 10.1103/PhysRevD.64.053018 PACS number(s): 12.15.Lk, 13.40.−f

I. INTRODUCTION

The projects to build high energy and high luminosity e^+e^- colliders [1,2] have recently motivated the study of the high energy behavior of the electroweak corrections to several e^+e^- annihilation processes. Explicit computations of the linear and quadratic logarithmic contributions to various observables have shown remarkable properties which should be largely observable at these future machines and should provide deep tests of the different sectors (gauge, matter, scalar) of the standard model (SM) as well as of its supersymmetric extensions, such as the minimal supersymmetric standard model (MSSM) [3,4]. In fact, for many years it has been known that in certain circumstances large logarithmic terms, in particular, quadratic logarithms, can appear [5,6]. The general features of the asymptotic one-loop electroweak corrections have been studied, a classification of the linear and quadratic logarithms has been established, some two-loop effects have been computed, and the possibility of resumming certain classes of contributions has been discussed [7–11].

On the other hand, the possibility of realizing high energy and high luminosity $\gamma\gamma$ collisions at e^+e^- colliders through the laser backscattering procedure is actively considered [12,13]. One already knows that electroweak radiative corrections to $\gamma\gamma \to f\bar{f}$ processes both in the SM [14] and in the MSSM [15] are sizable enough to be observable owing to the large luminosities expected at these machines, which should allow one to reach an accuracy better than the percent level.

The purpose of the present paper is to report on a study of the high energy behavior of the electroweak corrections to the process $\gamma\gamma \to f\bar{f}$ in the SM and the MSSM, performed along the same lines as those taken for the aforementioned studies of the $e^+e^- \to f\bar{f}$ processes. We will show that the $\gamma\gamma \to f\bar{f}$ processes offer an independent way to check the general properties of the asymptotic logarithmic terms originating from the various sectors of the electroweak interactions, and we will give precise numerical illustrations in order to see how they can be experimentally tested. A great similarity with the properties of the $e^+e^- \to f\bar{f}$ processes will appear and will allow us to conclude that $\gamma\gamma \to f\bar{f}$ processes can equally well contribute to the tests of the SM at high energies and to the search for its possible modifications or extensions.

The contents of the paper are as follows. In Sec. II we present the dynamical content of the SM and MSSM and we proceed with the computation of the complete one-loop weak contributions in the asymptotic regime. QED and QCD corrections are left aside as they depend on the detection conditions and are usually included in specific Monte Carlo programs [14]. After having checked that the set of self-energy, vertex, and box diagrams that are retained in the high energy limit is gauge independent and satisfies photon current conservation, we systematically work in the $\xi=1$ gauge. We check the convergence of the separate contributions of the various sectors (neutral gauge, charged gauge, Yukawa) of the standard model, as well as of the additional supersymmetry (SUSY) terms (gaugino, Higgsino, additional Higgs bosons). We keep the single and the quadratic logarithmic contributions. We separate the angular independent corrections from the angular dependent ones. All these contributions are specified for the helicity amplitudes of the process $\gamma\gamma \to f\bar{f}$; they are explicitly given in analytical form in Appendixes A and B. From these expressions it is then easy to compute the various parts of the fully polarized $\gamma\gamma$ cross section. This is what we present in Sec. III. We then compute the effects on the various $\gamma\gamma$ observables and we present and discuss the results in the SM and MSSM cases. With the expected luminosity of the Linear Collider (LC) and CERN Linear Collider (CLIC) these various contributions should be experimentally observable. We then discuss the physics implications of the results as well as the domain of validity of the one-loop computation and the need for a two-loop computation or a resummation at very high energies. This output is summarized in the concluding Sec. IV.

II. DYNAMICAL ONE-LOOP CONTENT OF $\gamma\gamma \to F\bar{F}$ AT HIGH ENERGY

We found it convenient to express all the results in terms of helicity amplitudes [16] $F_{\lambda,\lambda',\tau,\tau'}$, $\lambda,\lambda',\tau,\tau'$ being the

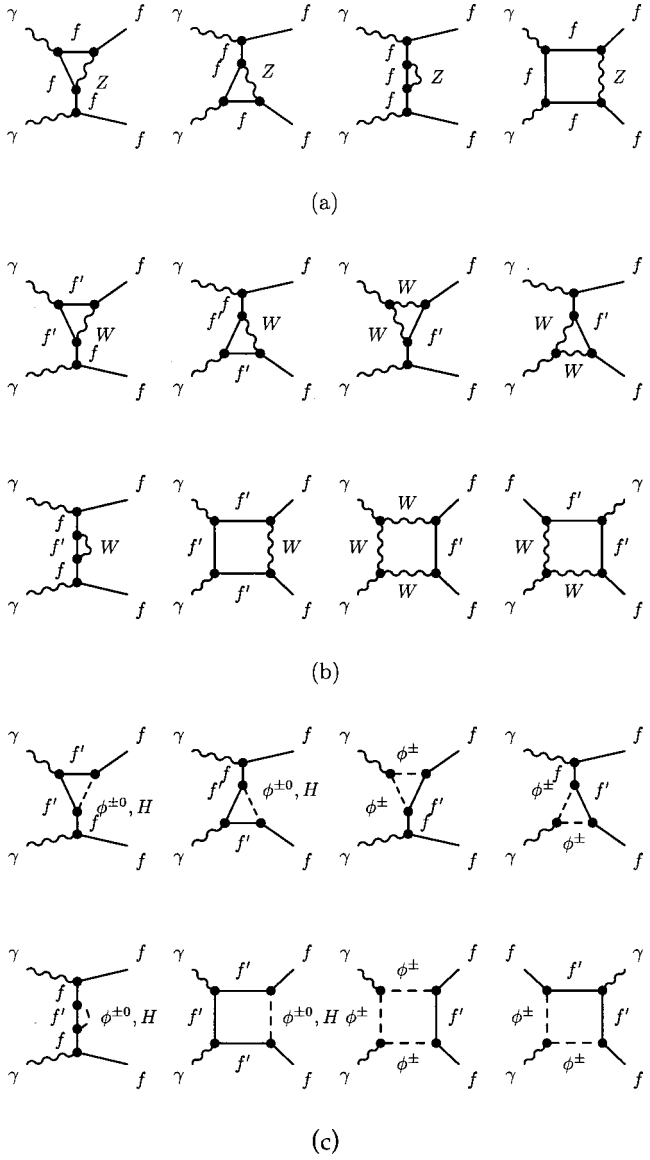

FIG. 1. SM diagrams contributing in the asymptotic regime of $\gamma\gamma\to f\bar{f}$, Z sector (a), W sector (b), and Higgs sector (c).

helicities of the two photons and of the fermion and antifermion, respectively; it is then easy to get the expressions of the observables in polarized photon-photon collisions. The Born term consists of two diagrams with fermion exchange in the t and u channels. It is $\gamma\gamma$ symmetric; its amplitude, in the high energy limit, is written in Appendix A. It only contributes to the $|\Delta\lambda|=2$ helicity amplitudes.

At one loop, the list of diagrams (to be symmetrized by interchanging the two photons) that contribute to the logarithmic terms in the high energy limit is given in Figs. 1(a–c) for the SM case. In the MSSM case, the additional SUSY diagrams can be found in Figs. 2(a,b). We have checked that these contributions are $(\xi-1)$ independent and that current conservation $(l^\mu J_\mu=0)$ holds separately for each photon. In Figs. 1(a–c) and 2(a,b) we have not drawn the external (photon, fermion) self-energy diagrams which do not contribute to the logarithmic terms, although they must be taken into account in order to get cancellation of the divergences gen-

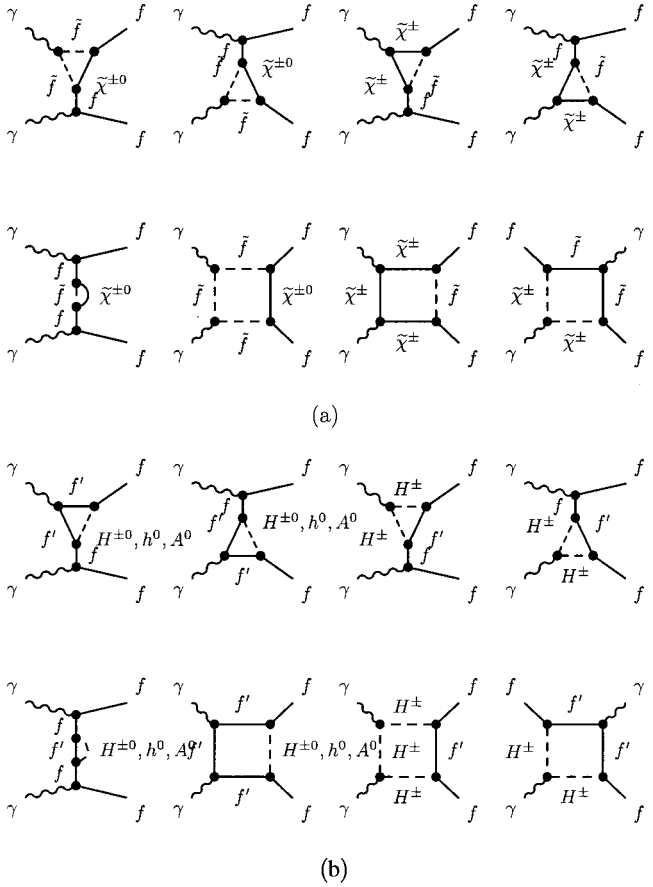

FIG. 2. SUSY additional diagrams contributing in the asymptotic regime of $\gamma\gamma\to f\bar{f}$; chargino and neutralino sector (a), and SUSY Higgs sector (b).

erated by the internal fermion self-energy and by the triangular diagrams; box diagrams are convergent.

The explicit expressions of the helicity amplitudes in the high energy limit are given separately for each sector of the electroweak corrections in an analytical form in Appendix A. They are obtained by deriving the complete expressions of the amplitudes in terms of Passarino-Veltman functions [17], and retaining only the asymptotic (logarithmic) parts of these functions (see Appendix B). In a second step we retain only the terms that contain linear ($\ln s$) and quadratic ($\ln^2 s$) logarithms, which we call *leading terms*, neglecting terms like $\ln(t/s)$, . . . , etc., which we call *nonleading terms*. During this procedure we checked that the divergences and the fermion mass singularities cancel. We also separated the coefficients of the leading logarithms that are θ independent from those that are θ dependent (θ is the c.m. scattering angle). We now discuss these various terms in turn.

Standard model corrections

γ and Z sectors

A first set of corrections is given by the internal fermion self-energy, triangle, and box diagrams of Fig. 1(a) containing one Z boson. The corresponding helicity amplitudes are given in Eqs. (A3) and (A4) (terms proportional to $[g^Z_{Vf}$

$-g^Z_{Af}(2\tau)]^2/4s^2_W c^2_W$). One can check in Eqs. (A5),(A6) that the leading terms of the $|\Delta\lambda|=2$ helicity amplitude combine in an angular independent factor proportional to $[\ln^2(s/M^2_Z) - 3\ln(s/M^2_Z)]$ multiplying the Born amplitude, in agreement with the general rule obtained in Refs. [10,11], and that the correction to the $|\Delta\lambda|=0$ amplitude vanishes.

A similar set of corrections would be provided by the UV photon sector (cut at scale M_Z), just replacing the internal Z by an internal γ in all the diagrams of Fig. 1(a). The result is given in Eqs. (A3) and (A4) (terms with Q^2_f instead of $[g^Z_{Vf} - g^Z_{Af}(2\tau)]^2/4s^2_W c^2_W$). The properties of this "γ sector" are exactly similar to those of the Z sector. In the following numerical discussions we shall omit it, taking the standpoint that all photonic corrections (UV and IR including soft photon emission) should be put together inside the QED-type corrections, which depend on the characteristics of the detectors and are generally treated separately by specific programs. This is obviously a matter of choice, which can easily be modified.

W sector

The corresponding diagrams are listed in Fig. 1(b). In addition to those obtained just by replacing the Z by the W, there now appear new triangle and box diagrams involving the three-boson γWW coupling. The resulting amplitudes are given in Eqs. (A7),(A8). One sees that the leading terms Eqs. (A9),(A10) are enriched by angular dependent and angular independent contributions arising from the γWW coupling, which appear in addition to the $[\ln^2(s/M^2_Z) - 3\ln(s/M^2_Z)]$ correction of the $|\Delta\lambda|=2$ amplitude.

Higgs sector

In the SM the Higgs sector consists in the set of diagrams of Fig. 1(c) involving charged and neutral $\Phi^{\pm,0}$ Goldstone bosons as well as the physical H Higgs boson, coupled to fermions through Yukawa terms proportional to m_f/M_W. This set of diagrams is relevant only for top and bottom quark production. The resulting amplitudes are given in Eqs. (A11),(A12) and their leading parts in Eqs. (A13),(A14). As expected from the general properties established in [10,11], these leading corrections coming from field renormalization constants (which one can directly obtain by considering only external self-energy contributions) are angular independent, linearly logarithmic, and affect only the $|\Delta\lambda|=2$ (Born) amplitude.

SUSY additional contributions

In the case of the MSSM, one should add to the previous SM terms the following additional SUSY corrections. We have separated them into two parts; first, a "nonmassive part" arising from the diagrams of Fig. 2(a), in which only the mass independent parts of the chargino and neutralino couplings are considered (corresponding to the charged or neutral "gaugino" components); secondly, a "massive part" due to the mass dependent terms of the chargino and neutralino couplings (corresponding to the charged or neutral "Higgsino" components) and also to the diagrams involving SUSY Higgs bosons (from this last contribution we have subtracted the contribution of the standard H_{SM} diagrams in order to avoid double counting of the physical Higgs sector). A general remark that was already made in the case of e^+e^- collisions is that, in the asymptotic regime $s \gg M^2$, the only dependence in the MSSM parameters that remains is the dependence on $\tan\beta$; all other parameters (except the global SUSY scale M appearing in the logarithmic terms) have disappeared because of the unitarity properties of the mixing matrices appearing in the SUSY couplings (see the fourth paper of Ref. [3]).

Nonmassive terms

The amplitudes resulting from the mass independent part of the diagrams of Fig. 2(a) are given in Eqs. (A15),(A16), and their leading terms in Eqs. (A17),(A18). For the same reason as in the case of the Higgs sector, the correction to the $|\Delta\lambda|=2$ amplitude is only linearly logarithmic and angular independent (they can also be obtained from the external self-energy contributions to the field renormalization constants), and the correction to the $|\Delta\lambda|=0$ amplitude vanishes asymptotically.

Massive terms

The amplitudes resulting from the mass dependent part of the diagrams of Fig. 2(a) and of Fig. 2(b) are given in Eqs. (A19),(A20), and their leading terms in Eqs. (A21),(A22). They behave asymptotically in a way similar to the SM Yukawa terms, the correction to the $|\Delta\lambda|=2$ amplitude being also only linearly logarithmic and angular independent, and the correction to the $|\Delta\lambda|=0$ amplitude vanishing. However, an important fact is the appearance of a $\cot^2\beta$ dependence in the term proportional to m^2_t/M^2_W, and a $\tan^2\beta$ dependence in the term proportional to m^2_b/M^2_W (which can be very important for large $\tan\beta$ values).

We also note that, in the MSSM, summing the SM and the additional SUSY contributions, the leading asymptotic massive terms combine in order to reproduce the massive SM contributions in which the m^2_t/M^2_W terms have been multiplied by $2(1+\cot^2\beta)$ and the m^2_b/M^2_W terms by $2(1+\tan^2\beta)$. This rule was already obtained for the process $e^+e^- \to f\bar{f}$ in the fifth paper of Ref. [3].

Let us finish this section by making a comparison with the asymptotic properties observed in the case of $e^+e^- \to f\bar{f}$. In the 't Hooft $\xi=1$ gauge, the contributions of the triangle and box contributions sometimes behave differently in the e^+e^- and in the $\gamma\gamma$ cases. The single Z and W triangles get only linear logarithms in the $\gamma\gamma$ case, whereas they get linear and quadratic logarithms in e^+e^-; in contrast, the WW triangle gets only a quadratic logarithm in $\gamma\gamma$ instead of the linear logarithm in e^+e^-. These differences are complemented by those of the box diagrams. In both Z and W sectors, the boxes produce linear and quadratic logarithms in $\gamma\gamma$, whereas in the e^+e^- case the ZZ box gives only linear logarithms and the WW box has both linear and quadratic logarithms. The Higgs and the SUSY sectors are very similar in the $\gamma\gamma$ and e^+e^- cases. They give only linear logarithms,

arising only from the triangle diagrams (and also from the internal fermion self-energy in the $\gamma\gamma$ case). The Higgs and SUSY box diagrams give no leading logarithms at all, in both $\gamma\gamma$ and e^+e^- cases.

III. EFFECTS ON THE $\gamma\gamma \to f\bar{f}$ OBSERVABLES

Having obtained the explicit expressions of the helicity amplitudes, it is easy to compute the various elements of the polarized $\gamma\gamma$ cross section. The general expression is given in Appendix C. Because of Bose statistics, CP invariance, and real (asymptotic) amplitudes, the expression of the cross section including terms up to order α^3 simplifies to

$$\begin{aligned}\frac{d\sigma}{d\tau\, d\cos\theta} = \frac{d\bar{L}_{\gamma\gamma}}{d\tau}\Bigg\{ & [1-\langle \xi_2\xi_2'\rangle]\frac{d\bar{\sigma}_0}{d\cos\theta} \\ & +[\langle \xi_2\rangle - \langle \xi_2'\rangle]\frac{d\bar{\sigma}_2}{d\cos\theta} \\ & +[\langle \xi_3\rangle \cos 2\phi + \langle \xi_3'\rangle \cos 2\phi']\frac{d\bar{\sigma}_3}{d\cos\theta} \\ & +[\langle \xi_3\xi_3'\rangle \cos 2(\phi+\phi')]\frac{d\bar{\sigma}_{33}}{d\cos\theta} \\ & +[\langle \xi_2\xi_3'\rangle \cos 2\phi' - \langle \xi_3\xi_2'\rangle \cos 2\phi]\frac{d\bar{\sigma}_{23}}{d\cos\theta}\Bigg\},\end{aligned} \tag{3.1}$$

in which $d\bar{L}_{\gamma\gamma}/d\tau$ describes the photon-photon luminosity per unit e^-e^+ flux obtained by the laser backscattering method [12]; $\tau = s/s_{ee}$ where $s \equiv s_{\gamma\gamma}$. The Stokes parameters (ξ_2, ξ_2'), (ξ_3, ξ_3'), and (ϕ, ϕ') describe, respectively, the average helicities, transverse polarizations, and azimuthal angles of the two backscattered photons (see Ref. [19]).

The Born amplitudes feed only the (parity conserving) $d\bar{\sigma}_0/d\cos\theta$ and $d\bar{\sigma}_{33}/d\cos\theta$ terms. The one-loop effects feed all the above terms. Note the specific photon polarization dependences, which can be used to test the structure of the one-loop electroweak corrections and the absence of unexpected effects. Taking into account the fact that

$$\frac{d\bar{\sigma}_0}{d\cos\theta}, \quad \frac{d\bar{\sigma}_3}{d\cos\theta}, \quad \frac{d\bar{\sigma}_{33}}{d\cos\theta}$$

are $\cos\theta$ *symmetric* and

$$\frac{d\bar{\sigma}_2}{d\cos\theta}, \quad \frac{d\bar{\sigma}_{23}}{d\cos\theta}$$

$\cos\theta$ *antisymmetric*, we construct the five ratios

$$R_0 = \int d\cos\theta \left[\frac{d\bar{\sigma}_0}{d\cos\theta} - \frac{d\bar{\sigma}_0^{Born}}{d\cos\theta}\right] \Big/ \int d\cos\theta \frac{d\bar{\sigma}_0^{Born}}{d\cos\theta}, \tag{3.2}$$

$$R_{33} = \int d\cos\theta \left[\frac{d\bar{\sigma}_{33}}{d\cos\theta} - \frac{d\bar{\sigma}_{33}^{Born}}{d\cos\theta}\right] \Big/ \int d\cos\theta \frac{d\bar{\sigma}_0^{Born}}{d\cos\theta}, \tag{3.3}$$

$$R_2 = \int_{F-B} d\cos\theta \left[\frac{d\bar{\sigma}_2}{d\cos\theta}\right] \Big/ \int d\cos\theta \frac{d\bar{\sigma}_0^{Born}}{d\cos\theta}, \tag{3.4}$$

$$R_3 = \int d\cos\theta \left[\frac{d\bar{\sigma}_3}{d\cos\theta}\right] \Big/ \int d\cos\theta \frac{d\bar{\sigma}_0^{Born}}{d\cos\theta}, \tag{3.5}$$

$$R_{23} = \int_{F-B} d\cos\theta \left[\frac{d\bar{\sigma}_{23}}{d\cos\theta}\right] \Big/ \int d\cos\theta \frac{d\bar{\sigma}_0^{Born}}{d\cos\theta}, \tag{3.6}$$

on which the electroweak effects are now illustrated and discussed.

One should first note, using the definitions of the various ''cross sections'' given in Appendix C, that the last two ratios R_3 and R_{23} only involve products of $|\Delta\lambda = 0|$ with $|\Delta\lambda = 2|$ amplitudes. As we have seen that, in the asymptotic regime (see, for example, the leading expressions written in Appendix A), the one-loop contributions to $|\Delta\lambda = 0|$ amplitudes are much weaker than those to $|\Delta\lambda = 2|$ amplitudes, one expects that these two ratios are much weaker than the other three.

Angular distributions

The angular distribution of the unpolarized Born cross section $d\sigma_0^{Born}/d\cos\theta$ is (symmetrically) strongly peaked in the forward and backward directions [see Figs. 3(a–c) at 3 TeV]. The electroweak corrections modify this distribution somewhat because their effect is larger in the central region, as shown in Figs. 4(a–c) where we plot the angular dependence of the relative effect of the electroweak corrections, defined as

$$\Delta\left(\frac{d\sigma_0}{d\cos\theta}\right) \equiv \left[\frac{d\sigma_0}{d\cos\theta} - \frac{d\sigma_0^{Born}}{d\cos\theta}\right] \Big/ \frac{d\sigma_0^{Born}}{d\cos\theta}. \tag{3.7}$$

It will therefore be interesting to have the largest possible angular acceptance allowed by experimental detection and to cut the angular distribution into several bins. One could then check the relative increase of the weak corrections in the central region.

Note that the radiative correction effect is always negative, that the supersymmetric corrections always increase the magnitude of the effect, and in the case of $t\bar{t}$, $b\bar{b}$ that this effect strongly depends on $\tan\beta$.

We now study in more detail the behavior of these effects versus the energy, by considering the integrated cross sections. In the following illustrations we choose to integrate the angular distributions in the domain $30° < \theta < 150°$.

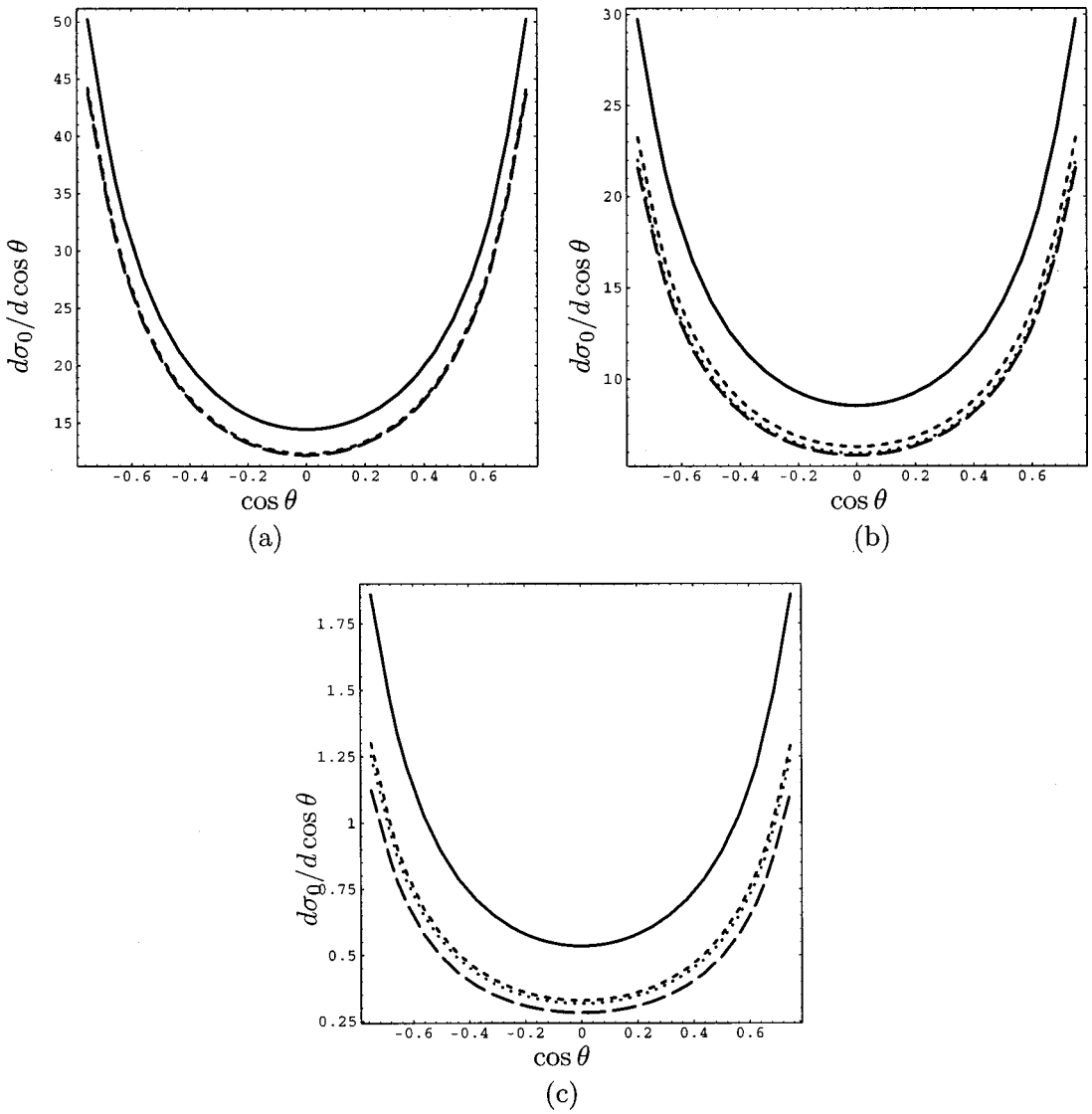

FIG. 3. Angular distribution of the unpolarized $\gamma\gamma \to f\bar{f}$ cross section at 3 TeV; l^+l^- (a), $t\bar{t}$ (b), $b\bar{b}$ (c); Born (solid), total SM (small dashed), total MSSM ($\tan\beta = 4$) (dotted), and total MSSM ($\tan\beta = 40$) (large dashed).

Leading versus nonleading terms

It is interesting to compare, as a function of the energy, the relative importance of the various logarithmic terms that were presented in the previous Section II. We will do that by considering the ratio R_0 giving the relative electroweak effects on the unpolarized cross section, defined in Eq. (3.2).

In Figs. 5(a,b) for l^+l^-, Figs. 6(a,b,c) for $t\bar{t}$, and Fig. 7(a,b,c) for $b\bar{b}$ we show, separately for the SM and the MSSM cases, the contribution of the sum of all logarithmic terms (collected in Appendixes A and B), compared to the results obtained when nonleading logarithmic terms are dropped [i.e., terms of the type $\ln^2(t/s)$, . . . , etc.,] and also to the results obtained when dropping, in addition, the leading angular dependent terms [terms $\ln(s/M^2)$ multiplied by angular dependent logarithms].

One sees that the nonleading logarithmic terms (which appear in the expressions of the box contributions given in Appendix B) behave roughly like an additional small constant contribution (of the order of 1%) whose relative importance as compared to the full electroweak correction decreases with the energy; this is true for both the SM and the MSSM cases.

On the contrary, the leading angular dependent terms (which appear in the triangle diagrams involving the γWW three-boson coupling) are more important (similar effects have been noticed in Ref. [11], in the case of the crossed channel $e^+e^- \to \gamma\gamma$) and increase with increasing energy. They cannot be omitted at all, and we will come back to their role in the final discussion. This comment applies to both the SM and the MSSM cases, as the SUSY additional contributions only consist of angular independent contributions.

We have checked that, around 1 TeV, our asymptotic results agree with those obtained in Ref. [14] for the purely weak part of the SM corrections to light fermion pair production. In the $t\bar{t}$ case, the agreement at 1 TeV is only qualitative, for both the SM case [14] and the MSSM case [15], as

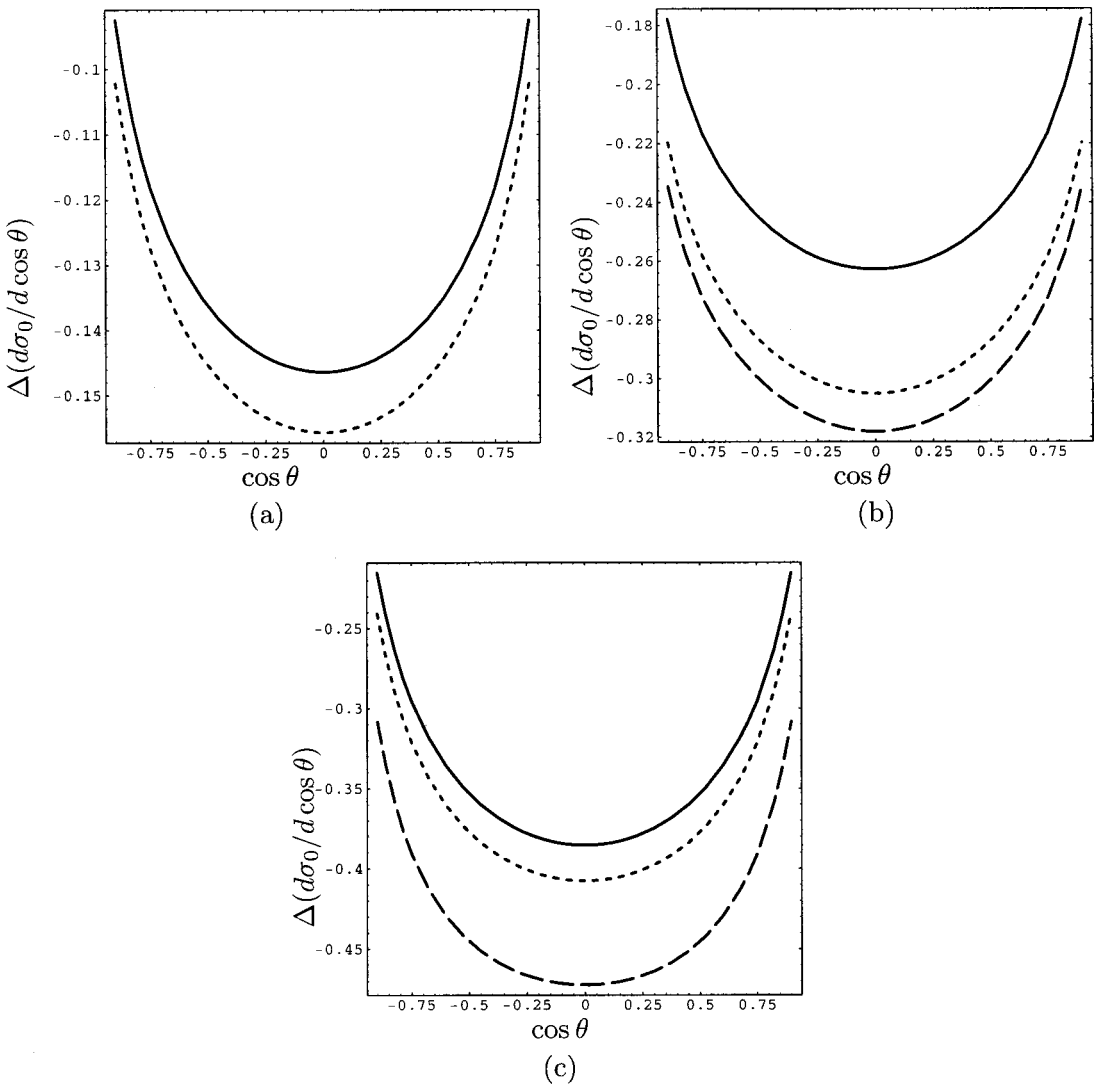

FIG. 4. Angular distribution of the relative departure from the unpolarized Born $\gamma\gamma\to f\bar{f}$ cross section at 3 TeV due to electroweak radiative corrections; l^+l^- (a), $t\bar{t}$ (b), $b\bar{b}$ (c); total SM (solid), total MSSM ($\tan\beta=4$) (small dashed), total MSSM ($\tan\beta=40$) (large dashed).

this energy is just marginally "asymptotic" for top quarks and for supersymmetric contributions. Nevertheless, the cancellation of the various MSSM parameters, except for the large $\tan\beta$ dependence that we emphasized, can already be seen at this energy in [15].

Importance of Yukawa terms

In Figs. 6(a,b,c) for $t\bar{t}$ and Figs. 7(a,b,c) for $b\bar{b}$, we have also shown the effect of dropping the Yukawa terms (coming from the Higgs and the Higgsino sectors) proportional to m_t^2/M_W^2 and m_b^2/M_W^2. Comparing the curves for the SM case and the curves for the case with no Yukawa terms in Fig. 6(a) for $t\bar{t}$ and Fig. 7(a) for $b\bar{b}$, one sees that these terms are very important, especially in the $t\bar{t}$ case, where they contribute easily half the effect at CLIC energies. In the MSSM case, the comparison is made in Figs. 6(b) and 7(b) for $\tan\beta=4$, and in Figs. 6(c) and 7(c) for $\tan\beta=40$. The $\tan\beta$ dependence can be understood by looking at Eq. (A21), in which one sees a $\cot^2\beta$ dependence associated with the term (m_t^2/M_W^2) and a $\tan^2\beta$ dependence associated with (m_b^2/M_W^2), which becomes dominant at very large $\tan\beta$ values. These properties are rather similar to those observed in $\gamma\gamma\to f\bar{f}$ [18].

Polarized and unpolarized cross sections versus the energy

We finally illustrate the behavior of the various terms of the polarized cross section, Eq. (3.1), versus the energy, in the l^+l^-, $t\bar{t}$, and $b\bar{b}$ cases.

In Figs. 8(a,b,c) and 9(a,b,c) we present the ratios R_0 and R_{33} which show the relative departures from the Born prediction [see Eqs. (3.2),(3.3)]. The effects are in all cases of the order of several percent at LC energies and of the order of 10–20 % at CLIC energies. In the MSSM case they are larger than in the SM case, especially for large $\tan\beta$ values.

In Figs. 10(a,b,c), 11(a,b,c), and 12(a,b,c) we present the ratios R_2, R_3, and R_{23} defined in Eqs. (3.4), (3.5), and (3.6).

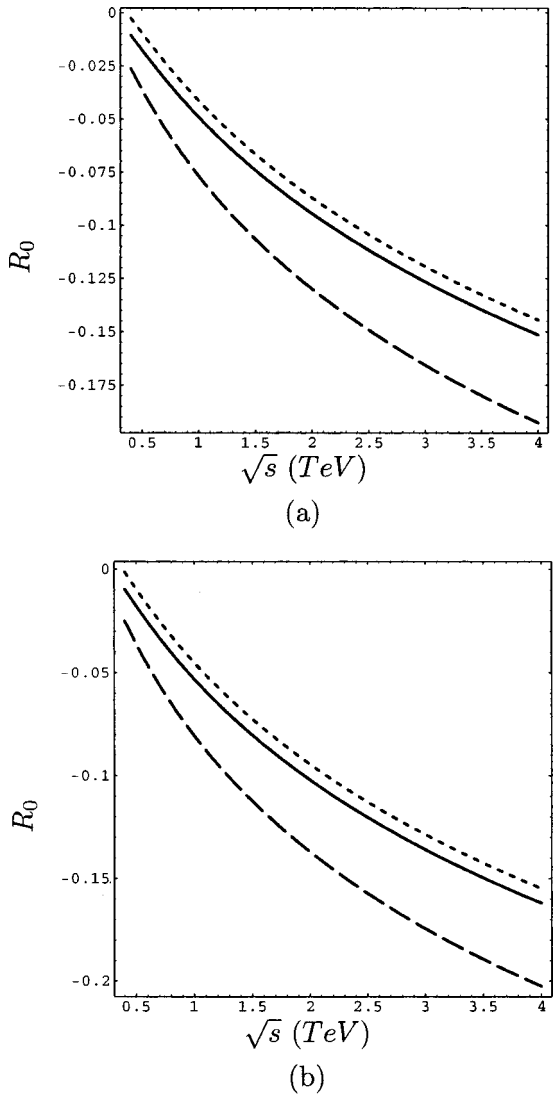

FIG. 5. The ratio R_0 for $\gamma\gamma \to l^+l^-$ versus the energy; SM (a), MSSM (b); all logarithmic terms (solid), leading terms only (small dashed), leading angular independent terms only (large dashed).

There is no Born contribution to these terms. The effects in R_2 (circular photon polarization dependence) are comparable to those previously seen in R_0. This is because R_2 measures the parity violating effects which are maximal in W couplings. On the contrary, the effects are very small in R_3 (one photon transversally polarized) and R_{23} (one photon transversally polarized, the other circularly polarized) because these terms, as we have already mentioned after their definitions, are proportional to the interference of small $\Delta\lambda = 0$ amplitudes [which have no leading $\ln(s/M^2)$ or $\ln^2(s/M^2)$ terms] with $\Delta\lambda = 2$ ones. Very high energies are required in order for these observables to reach the observable percent level.

We can add a final remark concerning the cross section for $\gamma\gamma$ to hadrons, the analog of the cross section for hadron production in e^+e^- collisions $\sigma_5 \equiv \sigma(e^+e^- \to u\bar{u} + c\bar{c} + d\bar{d} + s\bar{s} + b\bar{b})$. In $\gamma\gamma$ collisions, as we can see from Figs. 3(b,c), because of the factor Q_f^4 in the Born cross section, the rate is largely dominated by the contribution of up quarks (u,c), and the Yukawa contribution, appearing solely in the b case, can be completely neglected. So the properties of the electroweak radiative corrections to $\sigma(\gamma\gamma \to \text{hadrons})$ can be totally inferred from those of $\sigma(\gamma\gamma \to t\bar{t})$, ignoring the Yukawa contributions; see, for example, the curves corresponding to the case with no Yukawa terms in Figs. 6(a,b).

IV. CONCLUSIONS

We have studied the high energy behavior of the one-loop weak corrections to the processes $\gamma\gamma \to f\bar{f}$, in the SM and the MSSM.

In the asymptotic energy regime, we have classified and computed all correction terms coming in the 't Hooft $\xi = 1$ gauge from fermion self-energies, triangle, and box diagrams. We have checked that, in each weak sector, the set of diagrams contributes in a gauge independent way to the linear and quadratic logarithmic contributions to the $\gamma\gamma \to f\bar{f}$ amplitudes. Explicit analytic expressions are given in Appendixes A and B, and turn out to be rather simple and reflect in a remarkable way the theoretical properties of the SM charged gauge, neutral gauge, and Higgs sectors and of the MSSM gaugino and Higgsino sectors. These results satisfy the known general properties of leading electroweak logarithms at one loop [7,10,11]. They also match with the complete one-loop computations performed around 1 TeV in [14,15].

We have shown that these effects should be well visible in $\gamma\gamma$ collisions at LC and CLIC, the large luminosities expected at these machines allowing one to reach an accuracy better than the percent level. We have given the results for five observables defined in the case of polarized photon beams. Clearly, the behavior of each observable should provide clean tests of the SM or the MSSM and allow us to check the absence of unexpected new physics effects.

An important fact is the strong rise of the effect on the cross section, partly due to the angular independent factor $\alpha/4\pi[\ln^2(s/M_W^2) - 3\ln(s/M_W^2)]$, but we have shown that there are also important angular dependent contributions. A clear difference also appears in each $f = l,t,b$ case between the SM and MSSM corrections. The SUSY additional terms increase the magnitude of the weak corrections. For example, at 3 TeV, in l^+l^- production, the correction is -12.7% in the SM and -13.6% in the MSSM. In the $t\bar{t}$ and $b\bar{b}$ cases, the Yukawa terms contribute for a large part of the effect, both in the SM and in the MSSM; in this last case an observable $\tan\beta$ dependence appears. At 3 TeV, the weak effects on $t\bar{t}$ production are -23.1% in the SM, -27.2% in MSSM ($\tan\beta = 4$), and -28.6% in MSSM ($\tan\beta = 40$); and for $b\bar{b}$ production, they are -32.3% in the SM, -34.8% in the MSSM ($\tan\beta = 4$), -41.6% in the MSSM ($\tan\beta = 40$). This $\tan\beta$ dependence could be used for a $\tan\beta$ measurement (see the corresponding discussion in e^+e^- collisions in Ref. [18]).

These results are complementary to those observed in the process $e^+e^- \to f\bar{f}$. We have shown that the roles of the

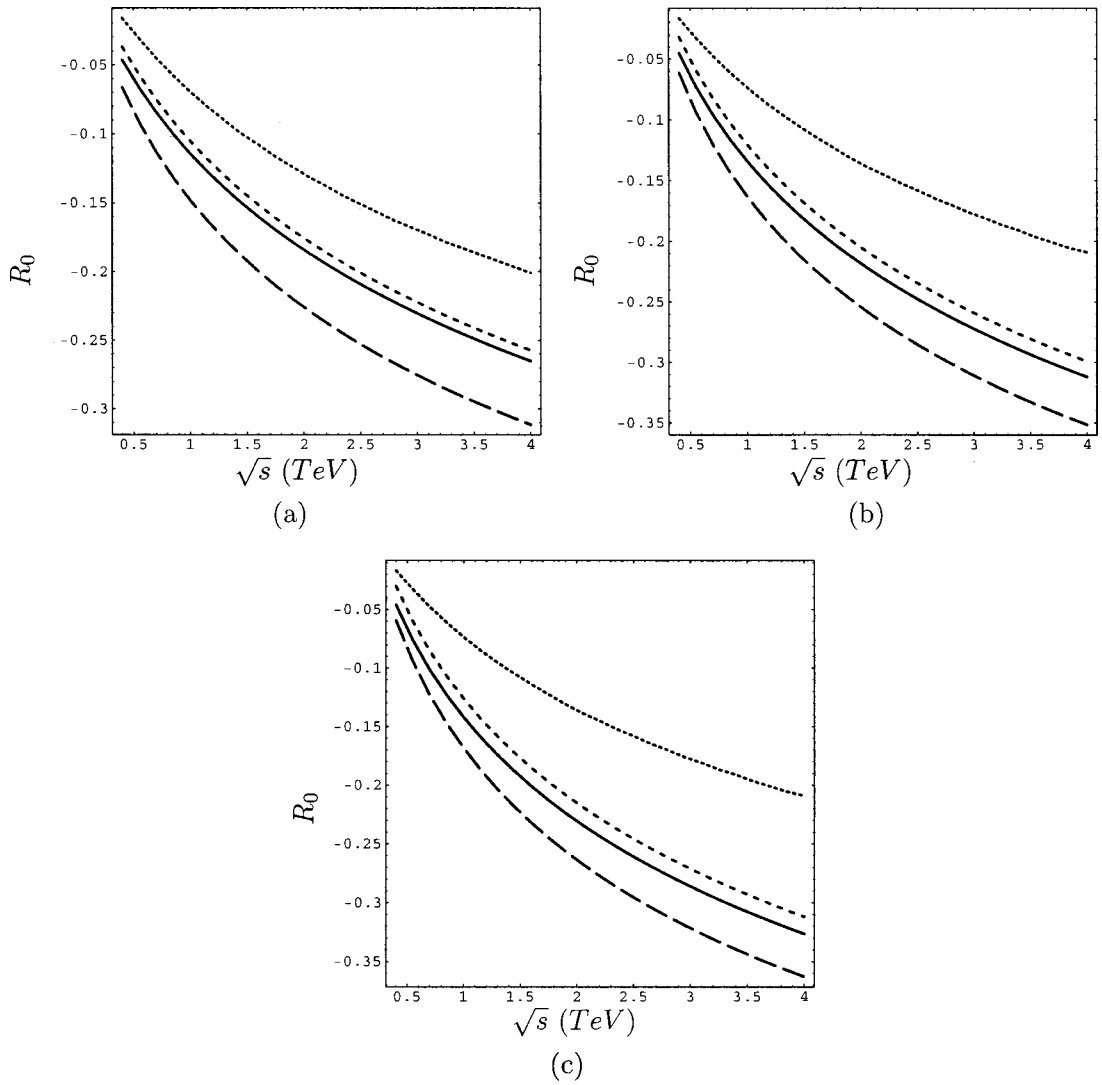

FIG. 6. The ratio R_0 for $\gamma\gamma \to t\bar{t}$ versus the energy; SM (a), MSSM ($\tan\beta=4$) (b); MSSM ($\tan\beta=40$) (c); all logarithmic terms (solid), leading terms only (small dashed), leading angular independent terms only (large dashed); all logarithmic without Yukawa terms (very small dashed).

self-energy, triangle, and box diagrams are different in the two processes, but the qualitative aspect of the information that can be reached about the features of the electroweak corrections is rather similar. There are, however, quantitative differences when comparing the effects in l^+l^-, $b\bar{b}$, and $t\bar{t}$ production. This is essentially due to the fact that in $\gamma\gamma$ collisions the Born term, proportional to Q_f^4, is especially small in the $b\bar{b}$ case, so that the electroweak corrections are relatively larger. Also the effects of gauge, Yukawa, and SUSY contributions are cumulative so that the corrections are larger than in the $e^+e^- \to f\bar{f}$ processes at the same energy.

As these first order effects already reach the 10% level around 1 TeV, and 30% around 3 TeV, one may naively expect that higher order terms easily reach the few percent level, observable at CLIC, raising the question of a possible two-loop computation. For the angular independent terms, general resummation techniques have been proposed [7–11], which would partly solve the problem. However, we have shown that there are important angular dependent terms for which no prescription has yet been obtained and may require an explicit two-loop computation.

At lower energies (the 0.5 to 1 TeV domain of LC), there is apparently no such problem. Although the effect in $\gamma\gamma \to b\bar{b}$ can reach 15% at 1 TeV, the weaker experimental accuracy in this channel may still allow one to stay at the one-loop level. However, as we have shown by comparing leading and nonleading logarithmic terms, in this energy range the logarithmic approximation is probably not sufficient. Constant terms (and possibly terms of order M^2/s) may not be negligible, especially if the SUSY scale is rather high, and one may not be allowed to neglect the mass of the SUSY particles running inside the loops. This approximation also fails to reproduce the ''resonance'' effects that appear around the thresholds for (sfermion or chargino) pair production [15]. In this ''low energy'' regime, the full set of MSSM

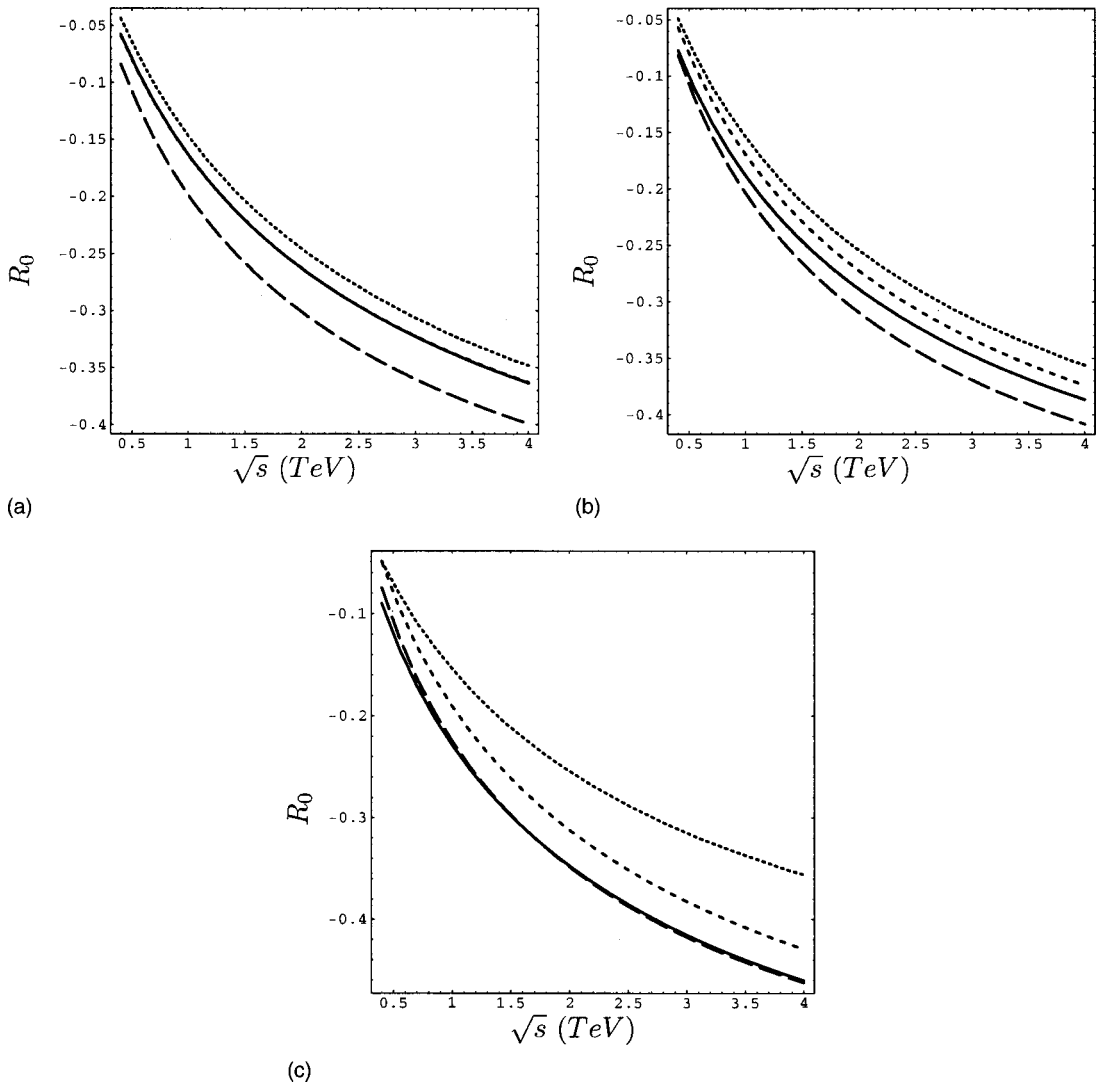

FIG. 7. The ratio R_0 for $\gamma\gamma \to b\bar{b}$ versus the energy; SM (a), MSSM ($\tan\beta = 4$) (b); MSSM ($\tan\beta = 40$) (c); all logarithmic terms (solid), leading terms only (small dashed), leading angular independent terms only (large dashed); all logarithmic without Yukawa terms (very small dashed).

parameters enters the game (and not only $\tan\beta$ as in the asymptotic regime). We intend to perform a detailed comparison of the logarithmic approximation with the exact computation of the full one-loop contributions. It should allow us to understand the role and discuss the measurability, in the LC regime, of each of the various MSSM parameters.

APPENDIX A: ASYMPTOTIC EXPRESSIONS OF THE HELICITY AMPLITUDES AT ONE LOOP

We denote by $F_{\lambda,\lambda',\tau,\tau'}$ the helicity amplitudes of the process $\gamma\gamma \to f\bar{f}$, $\lambda,\lambda',\tau,\tau'$ being the helicities of the photons (± 1), and of the fermion and antifermion ($\pm 1/2$) in the $\gamma\gamma$ center of mass. We denote by e,l, e',l' the photon polarization vectors and four-momenta and p,p' the fermion and antifermion four-momenta; $q = p - l = l' - p'$, $q' = p - l' = l - p'$; $\sqrt{s}$ and θ are the energy and the scattering angle.

We work in the high energy limit $s = (l+l')^2 = (p+p')^2$, $t = q^2 = -s/2(1-\cos\theta)$, $u = q'^2 = -s/2(1+\cos\theta) \gg M^2$ (avoiding the forward and backward domains), keeping only logarithmic terms involving s, t, or u. A general consequence of the high energy limit is the dominance of chirality conserving terms with $\tau' = -\tau$ only.

Born term

At high energy, the invariant amplitude corresponding to the diagrams of Fig. 1 is

$$\mathcal{R}^{Born} = -e^2 Q_f^2 \bar{u_f}(p)\left[\frac{\not e \not l \not e'}{t} + \frac{\not e' \not l' \not e}{u}\right] v_{\bar{f}}(p'). \quad \text{(A1)}$$

Q_f is the fermion charge in unit of $|e|$.

It leads to the helicity amplitudes

$$F^{Born}_{\lambda,-\lambda,\tau,-\tau} = -8\pi\alpha Q_f^2\left[\frac{\lambda + 2\tau\cos\theta}{\sin\theta}\right]. \quad \text{(A2)}$$

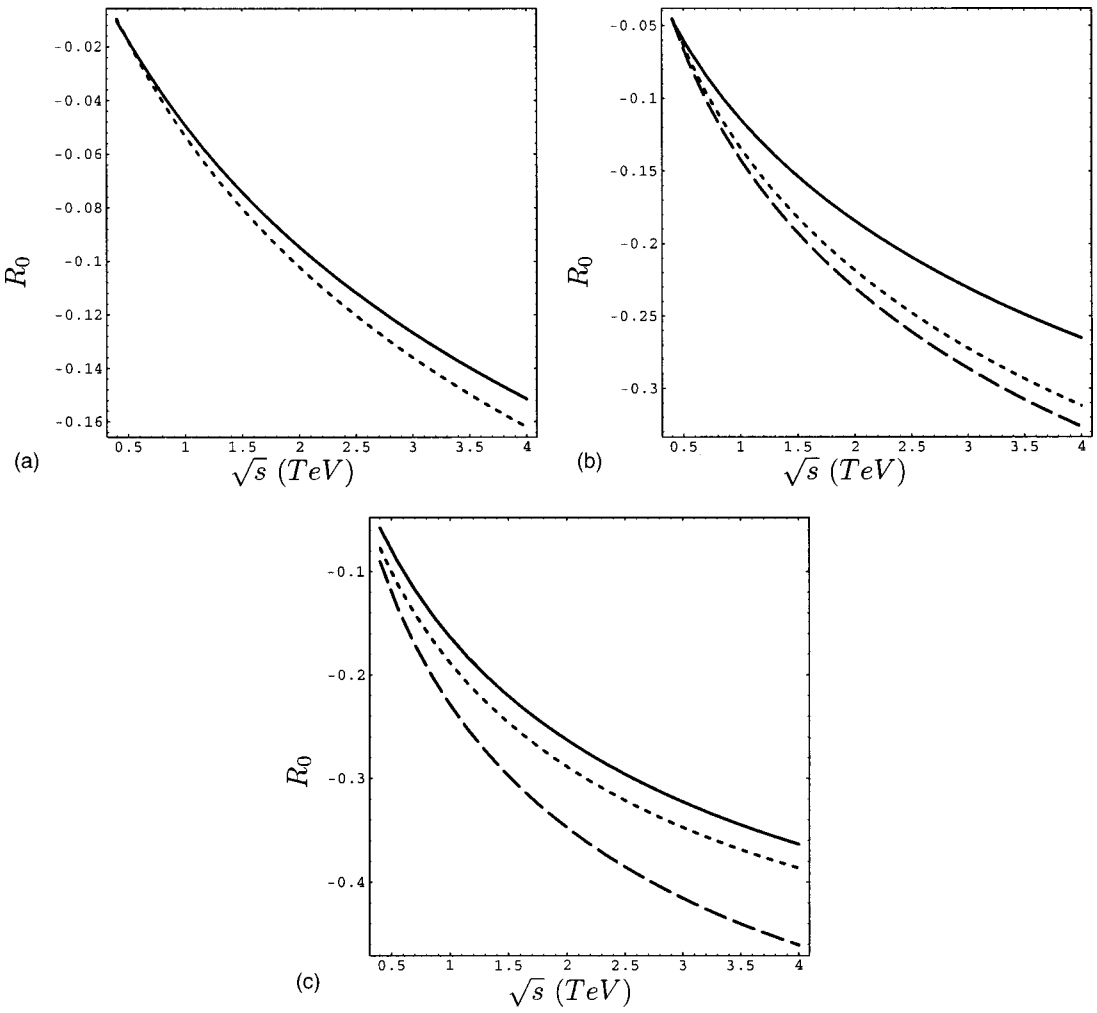

FIG. 8. The ratio R_0 for $\gamma\gamma\to f\bar{f}$ versus the energy; l^+l^- (a), $t\bar{t}$ (b), $b\bar{b}$ (c); SM (solid), MSSM ($\tan\beta=4$) (small dashed), MSSM ($\tan\beta=40$) (large dashed).

Note that at high energy, due to Bose symmetry, the Born term involves only $\lambda'=-\lambda$ (i.e. $|\Delta\lambda|=2$) amplitudes.

SM electroweak corrections

γ and Z sectors

The sum of self-energy, triangle, and box diagrams of Fig. 1(a) (to which external fermion self-energy diagrams are added) is convergent and gives the asymptotic contributions

$$F_{\lambda,-\lambda,\tau,-\tau}=\alpha^2Q_f^2\left\{Q_f^2+\frac{[g_{Vf}^Z-g_{Af}^Z(2\tau)]^2}{4s_W^2c_W^2}\right\}\times\left\{2\left[\frac{\lambda+(2\tau)\cos\theta}{\sin\theta}\right]\ln\frac{s}{M_Z^2}+B^1_{\lambda,-\lambda}(M_Z^2)\right\},\tag{A3}$$

$$F_{\lambda,\lambda,\tau,-\tau}=\alpha^2Q_f^2\left\{Q_f^2+\frac{[g_{Vf}^Z-g_{Af}^Z(2\tau)]^2}{4s_W^2c_W^2}\right\}\times\left\{-8\left[\frac{(2\tau)\cos\theta}{\sin\theta}\right]\ln\frac{s}{M_Z^2}+B^1_{\lambda,\lambda}(M_Z^2)\right\}.\tag{A4}$$

The box quantities B^i are defined in Appendix B, and $g_{Vf}^Z=I_{3f}(1-4s_W^2|Q_f|)$, $g_{Af}^Z=I_{3f}$.

The leading terms are

$$F^{l.t.}_{\lambda,-\lambda,\tau,-\tau}\to-F^{Born}_{\lambda,-\lambda,\tau,-\tau}\left(\frac{\alpha}{4\pi}\right)\left\{Q_f^2+\frac{[g_{Vf}^Z-g_{Af}^Z(2\tau)]^2}{4s_W^2c_W^2}\right\}\times\left(\ln^2\frac{s}{M_Z^2}-3\ln\frac{s}{M_Z^2}\right),\tag{A5}$$

$$F^{l.t.}_{\lambda,\lambda,\tau,-\tau}\to 0.\tag{A6}$$

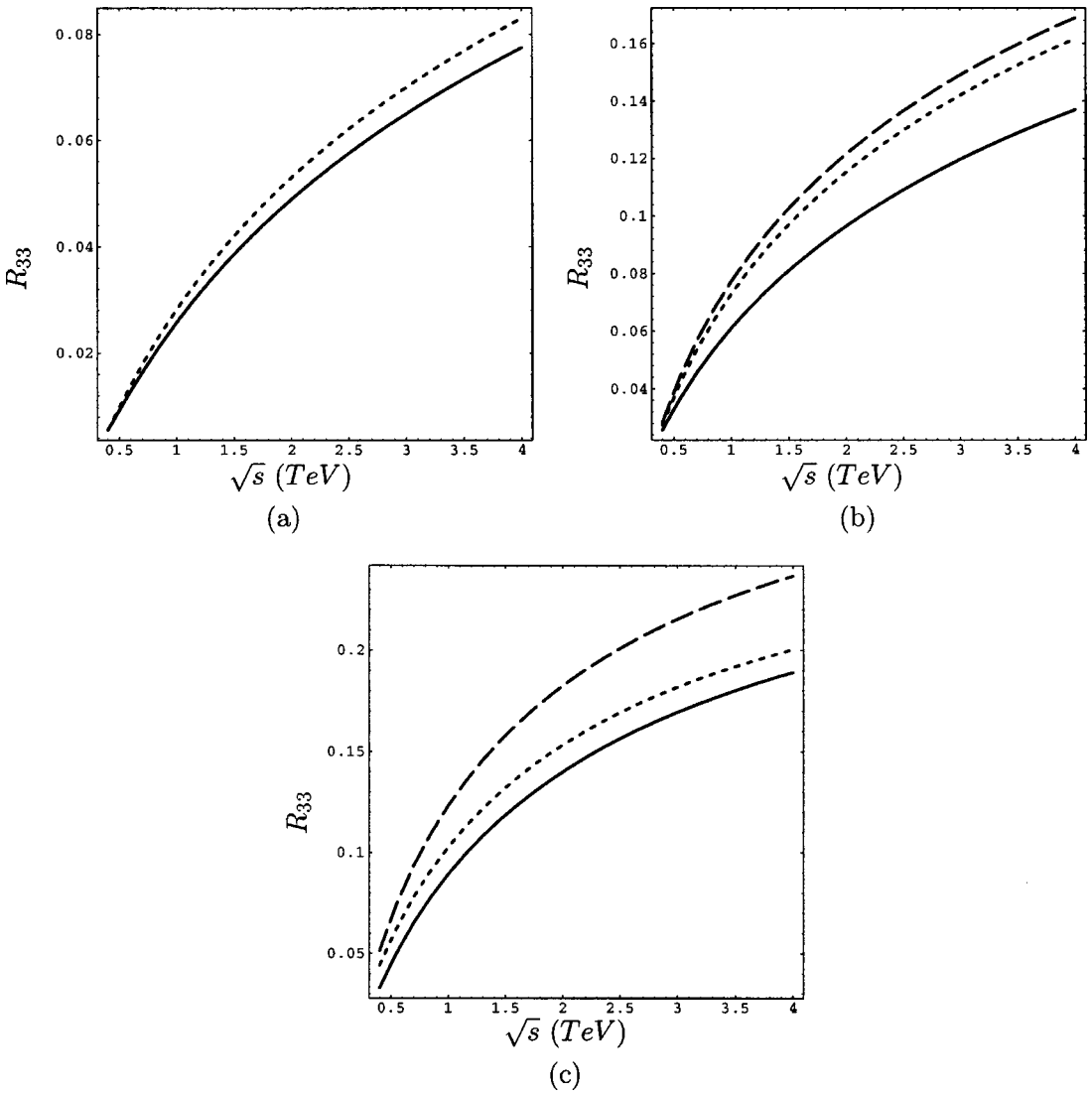

FIG. 9. The ratio R_{33} for $\gamma\gamma \to f\bar{f}$ versus the energy; l^+l^- (a), $t\bar{t}$ (b), $b\bar{b}$ (c); SM (solid), MSSM ($\tan\beta=4$) (small dashed), MSSM ($\tan\beta=40$) (large dashed).

W sector

We now sum the contributions of the charged gauge sector, with the self-energy, triangle, and box diagrams of Fig. 1(b). Note that in order to get a convergent result one has to add the photon self-energy contribution; it cancels the divergent contribution that appears in the axial term of the corrected γff vertex, whereas a remaining divergence in the vector term is absorbed by the charge renormalization:

$$F_{\lambda,-\lambda,\tau,-\tau}=\frac{\alpha^2}{4s_W^2}[1-(2\tau)]\Bigg\{\left[\frac{\lambda+(2\tau)\cos\theta}{\sin\theta}\right]\times\Bigg[2Q_f[Q_f-2(2I_{3f})]\ln\frac{s}{M_W^2}+Q_f(2I_{3f})\times\left((1+\cos\theta)\ln^2\frac{t}{m_W^2}+(1-\cos\theta)\ln^2\frac{u}{m_W^2}\right)+2\sin^2\theta\ln\frac{s}{M_W^2}\Bigg]+[Q_f-(2I_{3f})]^2B^1_{\lambda,-\lambda}(M_W^2)+B^2_{\lambda,-\lambda}(M_W^2)-[Q_f-(2I_{3f})]\times(2I_{3f})B^5_{\lambda,-\lambda}(M_W^2)\Bigg\}, \tag{A7}$$

$$F_{\lambda,\lambda,\tau,-\tau}=\frac{\alpha^2}{4s_W^2}[1-(2\tau)]\times\Bigg\{(2\tau)\Bigg[-8Q_f[Q_f-(2I_{3f})]\frac{\cos\theta}{\sin\theta}\ln\frac{s}{M_W^2}+Q_f(2I_{3f})\sin\theta\left(\frac{(2-\cos\theta)}{1-\cos\theta}\ln^2\frac{t}{m_W^2}-\frac{(2+\cos\theta)}{1+\cos\theta}\ln^2\frac{u}{m_W^2}\right)(-2\sin\theta\cos\theta)\ln\frac{s}{M_W^2}\Bigg]$$

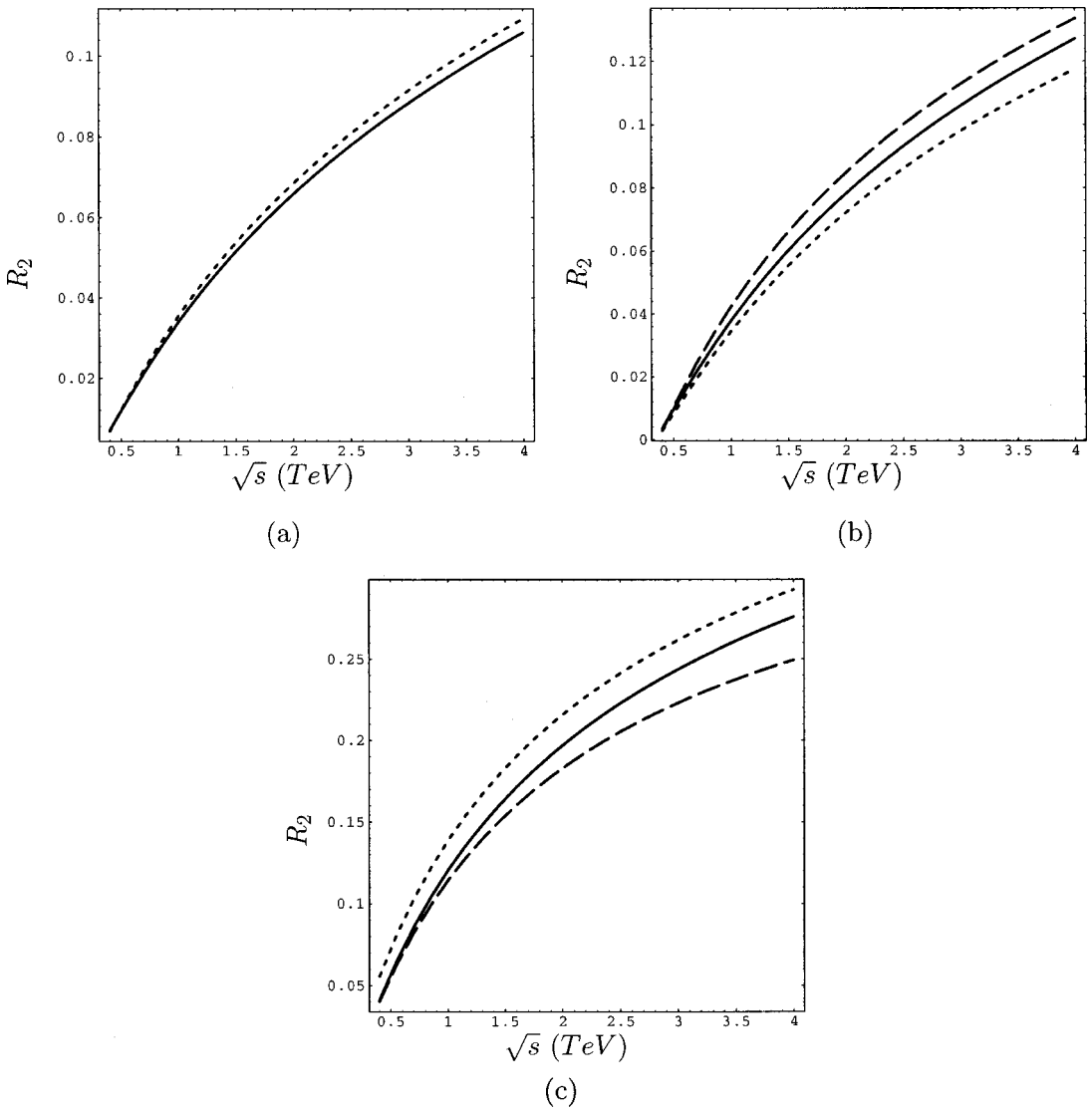

FIG. 10. The ratio R_2 for $\gamma\gamma \to f\bar{f}$ versus the energy; l^+l^- (a), $t\bar{t}$ (b), $b\bar{b}$ (c); SM (solid), MSSM ($\tan\beta=4$) (small dashed), MSSM ($\tan\beta=40$) (large dashed).

$$+[Q_f-(2I_{3f})]^2 B^1_{\lambda,\lambda}(M_W^2)+B^2_{\lambda,\lambda}(M_W^2)$$
$$-[Q_f-(2I_{3f})](2I_{3f})B^5_{\lambda,\lambda}(M_W^2)\Big\}. \qquad \text{(A8)}$$

The leading terms are

$$F^{l.t.}_{\lambda,-\lambda,\tau,-\tau} \to -F^{Born}_{\lambda,-\lambda,\tau,-\tau}\left(\frac{\alpha}{32\pi s_W^2 Q_f^2}\right)[1-(2\tau)]$$
$$\times\Big\{2Q_f^2\left(\ln^2\frac{s}{M_W^2}-3\ln\frac{s}{M_W^2}\right)$$
$$+4Q_f(2I_{3f})\ln^2\frac{s}{M_W^2}+4\Big[\cos\theta\ln\frac{1-\cos\theta}{1+\cos\theta}$$
$$+[2Q_f(2I_{3f})-1]\ln\frac{\sin^2\theta}{4}\Big]\ln\frac{s}{M_W^2}\Big\}, \qquad \text{(A9)}$$

$$F^{l.t.}_{\lambda,\lambda,\tau,-\tau} \to 0. \qquad \text{(A10)}$$

Note the appearance of angular dependent leading terms. This is the only sector where it happens (such terms were also found in Ref. [11] in the crossed channel $e^+e^- \to \gamma\gamma$ for left-handed electrons). See the discussion in Secs. II and III.

Higgs sector

We now add the contributions of the diagrams of Fig. 1(c) involving the Goldstone boson Φ and the physical Higgs boson H_{SM}. This concerns only the production of massive quarks $f=t,b$, as these contributions, arising from the Yukawa couplings, are proportional to m_f^2/M_W^2:

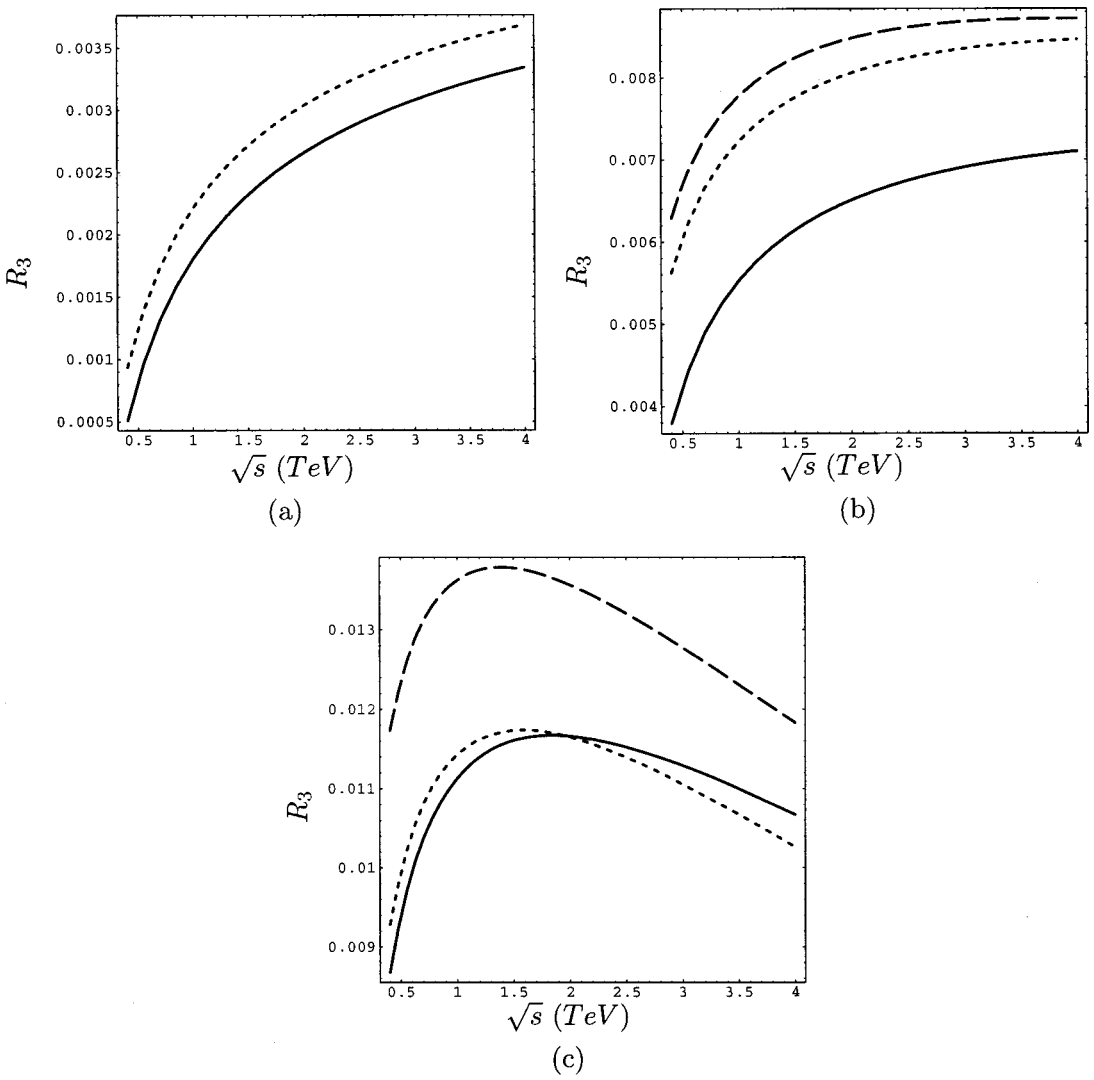

FIG. 11. The ratio R_3 for $\gamma\gamma \to f\bar{f}$ versus the energy; l^+l^- (a), $t\bar{t}$ (b), $b\bar{b}$ (c); SM (solid), MSSM ($\tan\beta=4$) (small dashed), MSSM ($\tan\beta=40$) (large dashed).

$$
\begin{aligned}
F_{\lambda,-\lambda,\tau,-\tau} = \frac{\alpha^2}{4s_W^2}\Bigg\{ & Q_f^2\left[\frac{\lambda+(2\tau)\cos\theta}{\sin\theta}\right] \\
& \times\left[\left(\frac{m_t^2}{M_W^2}[1+(2\tau)(2I_{3f})] + \frac{m_b^2}{M_W^2}[1-(2\tau)(2I_{3f})]\right) + 2\left(\frac{m_f^2}{M_W^2}\right)\right]\ln\frac{s}{M_W^2} + \{B^4_{\lambda,-\lambda} + [Q_f-(2I_{3f})]^2 \\
& \times B^3_{\lambda,-\lambda} - [Q_f-(2I_{3f})](2I_{3f})B^6_{\lambda,-\lambda}\} \\
& \times\left(\frac{m_t^2}{M_W^2}[1+(2\tau)(2I_{3f})] + \frac{m_b^2}{M_W^2}[1-(2\tau)(2I_{3f})]\right) \\
& + 2Q_f^2\left(\frac{m_f^2}{M_W^2}\right)B^3_{\lambda,-\lambda}\Bigg\}, \qquad \text{(A11)}
\end{aligned}
$$

$$
\begin{aligned}
F_{\lambda,\lambda,\tau,-\tau} = \frac{\alpha^2}{4s_W^2}\Bigg\{ & \{B^4_{\lambda,\lambda} + [Q_f-(2I_{3f})]^2 B^3_{\lambda,\lambda} \\
& - [Q_f-(2I_{3f})](2I_{3f})B^6_{\lambda,\lambda}\} \\
& \times\left[\frac{m_t^2}{M_W^2}[1+(2\tau)(2I_{3f})] + \frac{m_b^2}{M_W^2}[1-(2\tau)(2I_{3f})]\right] + 2Q_f^2\left(\frac{m_f^2}{M_W^2}\right)B^3_{\lambda,\lambda}\Bigg\}. \qquad \text{(A12)}
\end{aligned}
$$

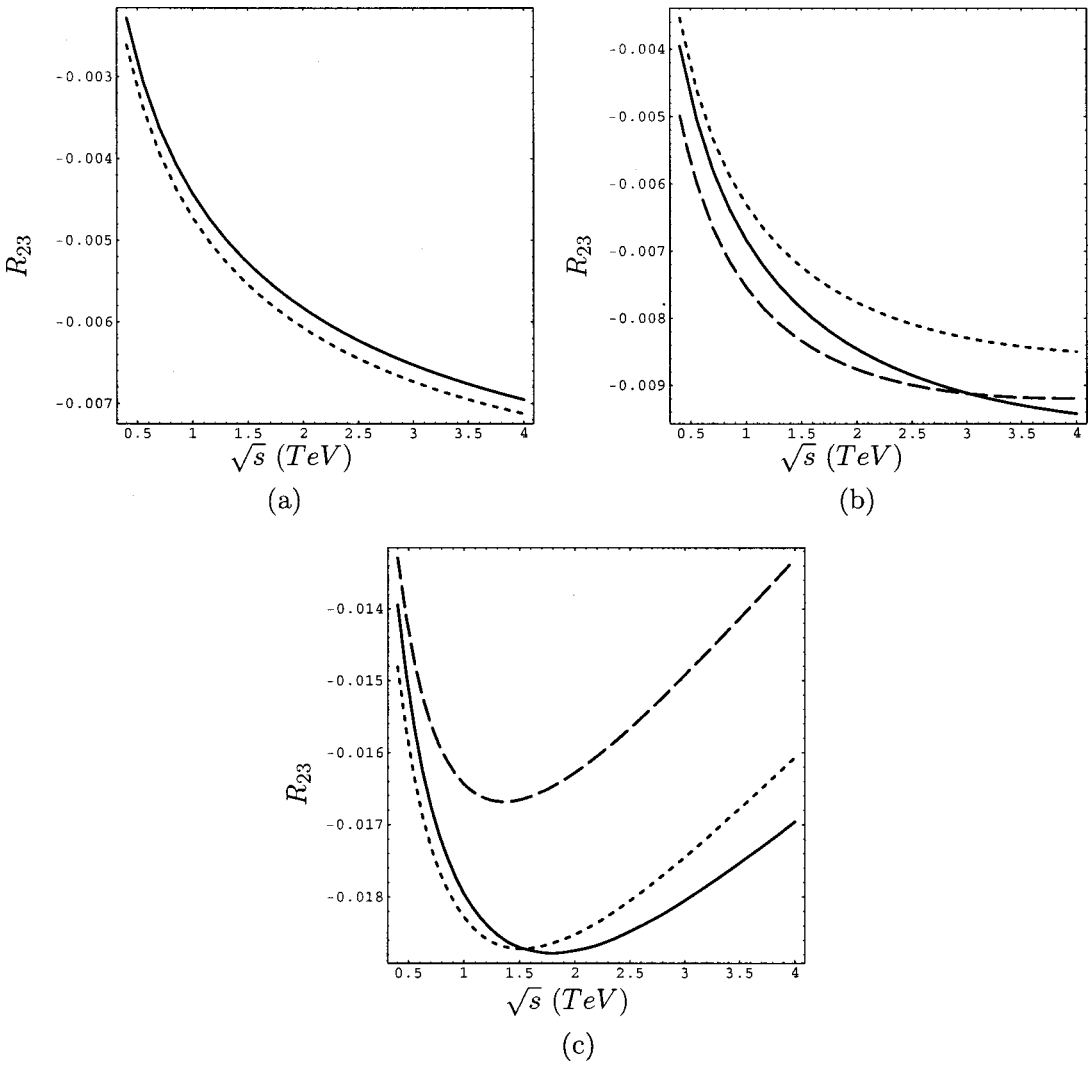

FIG. 12. The ratio R_{23} for $\gamma\gamma\to f\bar{f}$ versus the energy; l^+l^- (a), $t\bar{t}$ (b), $b\bar{b}$ (c); SM (solid), MSSM ($\tan\beta=4$) (small dashed), MSSM ($\tan\beta=40$) (large dashed).

The leading terms are

$$F^{l.t.}_{\lambda,-\lambda,\tau,-\tau}\to -F^{Born}_{\lambda,-\lambda,\tau,-\tau}\left(\frac{\alpha}{32\pi s_W^2}\right)\left\{\left(\frac{m_t^2}{M_W^2}[3+(2\tau)]+\frac{m_b^2}{M_W^2}[1-(2\tau)]\right)\delta_{tf}+\left(\frac{m_b^2}{M_W^2}[3+(2\tau)]+\frac{m_t^2}{M_W^2}[1-(2\tau)]\right)\delta_{bf}\right\}\ln\frac{s}{M_W^2}, \tag{A13}$$

$$F^{l.t.}_{\lambda,\lambda,\tau,-\tau}\to 0. \tag{A14}$$

Note that the box functions $B^{3,4,6}$ (and consequently the full Higgs contribution to $F_{\lambda,\lambda,\tau,-\tau}$) do not contribute to the leading $\ln s$ or $\ln^2 s$ terms; so no scale is mentioned in their notation (see Appendix B); the same property holds in the following supersymmetric contributions.

SUSY additional contributions

Nonmassive terms

By nonmassive terms we mean the contributions due to the diagrams involving gauge couplings of sfermions, charginos, and neutralinos. They come from self-energy, triangle, and box diagrams in Fig. 2(a) (and external fermion self-energy terms):

$$\begin{aligned}F_{\lambda,-\lambda,\tau,-\tau}=\frac{\alpha^2}{4s_W^2}\Bigg\{&\left[\frac{\lambda+(2\tau)\cos\theta}{\sin\theta}\right]\\&\times\left[2Q_f^2\left(\frac{2C_fQ_f^2}{c_W^2}+1-(2\tau)\right)\right]\ln\frac{s}{M^2}\\&+[1-(2\tau)]\{2B^3_{\lambda,-\lambda}-2[Q_f-(2I_{3f})](2I_{3f})\\&\times B^6_{\lambda,-\lambda}+D_fB^4_{\lambda,-\lambda}\}\\&+[1+(2\tau)]E_fB^4_{\lambda,-\lambda}\Bigg\},\end{aligned} \tag{A15}$$

$$F_{\lambda,\lambda,\tau,-\tau}=\frac{\alpha^2}{4s_W^2}([1-(2\tau)]\{2B^3_{\lambda,\lambda}-2[Q_f-(2I_{3f})]\times(2I_{3f})B^6_{\lambda,\lambda}+D_fB^4_{\lambda,\lambda}\}+[1+(2\tau)]E_fB^4_{\lambda,\lambda}), \tag{A16}$$

where

$$C_l=\frac{1}{4}[1-(2\tau)]+s_W^2[1+(2\tau)],\quad D_l=\frac{1}{c_W^2},\quad E_l=\frac{4s_W^2}{c_W^2},$$

$$C_t=\frac{9-8s_W^2}{36}[1-(2\tau)]+\frac{4s_W^2}{9}[1+(2\tau)],$$

$$D_t=\frac{2}{9}+\frac{4(9-8s_W^2)}{81c_W^2},\quad E_t=\frac{64s_W^2}{81c_W^2},$$

$$C_b=\frac{9-8s_W^2}{36}[1-(2\tau)]+\frac{s_W^2}{9}[1+(2\tau)],$$

$$D_b=\frac{8}{9}+\frac{(9-8s_W^2)}{81c_W^2},\qquad E_b=\frac{4s_W^2}{81c_W^2}.$$

The leading terms are

$$F^{l.t.}_{\lambda,-\lambda,\tau,-\tau}\to -F^{Born}_{\lambda,-\lambda,\tau,-\tau}\left(\frac{\alpha}{16\pi s_W^2}\right)\times\left[\left(\frac{2C_fQ_f^2}{c_W^2}+1-(2\tau)\right)\right]\ln\frac{s}{M^2}, \tag{A17}$$

$$F_{\lambda,\lambda,\tau,-\tau}\to 0. \tag{A18}$$

M is a common SUSY scale introduced for convenience (which is fixed to 0.5 TeV in the illustrations). Note that a change of value of M amounts to the introduction of additional (neglected) constant terms, as the SUSY contributions only appear with $\ln(s/M^2)$ and never with quadratic logarithmic terms.

Note in addition that the SUSY contribution to $F_{\lambda,\lambda,\tau,-\tau}$ also has no leading $\ln s$ or $\ln^2 s$ terms.

Massive terms

These terms arise from the Yukawa couplings of the Higgsino component of the charginos and neutralinos interacting with sfermions, as well as from the physical SUSY Higgs contributions (from which we subtract the SM Higgs contribution in order to avoid make double counting of the Higgs sector contribution). From self-energy, triangle, and box diagrams of Figs. 2(a,b) (and external fermion self-energy terms) one gets

$$\begin{aligned}F_{\lambda,-\lambda,\tau,-\tau}=\frac{\alpha^2}{4s_W^2}\Bigg\{&Q_f^2\left[\frac{\lambda+(2\tau)\cos\theta}{\sin\theta}\right]\Bigg[\left(\frac{m_t^2}{M_W^2}[1+(2\tau)(2I_{3f})](1+2\cot^2\beta)+\frac{m_b^2}{M_W^2}[1-(2\tau)(2I_{3f})](1+2\tan^2\beta)\right)\\&+2\left(\frac{m_f^2}{M_W^2}\right)[(1+2\cot^2\beta)\delta_{tf}+(1+2\tan^2\beta)\delta_{bf}]\Bigg]\ln\frac{s}{M^2}\\&+\{B^4_{\lambda,-\lambda}+[Q_f-(2I_{3f})]^2B^3_{\lambda,-\lambda}\}\left(\frac{m_t^2}{M_W^2}[1+(2\tau)(2I_{3f})]\cot^2\beta+\frac{m_b^2}{M_W^2}[1-(2\tau)(2I_{3f})]\tan^2\beta\right)\\&+\{B^3_{\lambda,-\lambda}+[Q_f-(2I_{3f})]^2B^4_{\lambda,-\lambda}\}\left(\frac{m_t^2}{M_W^2}[1+(2\tau)(2I_{3f})](1+\cot^2\beta)+\frac{m_b^2}{M_W^2}[1-(2\tau)(2I_{3f})](1+\tan^2\beta)\right)\\&-[Q_f-(2I_{3f})](2I_{3f})B^6_{\lambda,-\lambda}\left(\frac{m_t^2}{M_W^2}[1+(2\tau)(2I_{3f})](1+2\cot^2\beta)+\frac{m_b^2}{M_W^2}[1-(2\tau)(2I_{3f})](1+2\tan^2\beta)\right)\\&+2Q_f^2\frac{m_f^2}{M_W^2}\{B^3_{\lambda,-\lambda}[\cot^2\beta\delta_{tf}+\tan^2\beta\delta_{bf}]+B^4_{\lambda,-\lambda}[(1+\cot^2\beta)\delta_{tf}+(1+\tan^2\beta)\delta_{bf}]\}\Bigg\},\end{aligned} \tag{A19}$$

$$\begin{aligned}F_{\lambda,\lambda,\tau,-\tau}=\frac{\alpha^2}{4s_W^2}\Bigg\{&(B^4_{\lambda,\lambda}+[Q_f-(2I_{3f})]^2B^3_{\lambda,\lambda})\left(\frac{m_t^2}{M_W^2}[1+(2\tau)(2I_{3f})]\cot^2\beta+\frac{m_b^2}{M_W^2}[1-(2\tau)(2I_{3f})]\tan^2\beta\right)\\&+\{B^3_{\lambda,\lambda}+[Q_f-(2I_{3f})]^2B^4_{\lambda,\lambda}\}\left(\frac{m_t^2}{M_W^2}[1+(2\tau)(2I_{3f})](1+2\cot^2\beta)+\frac{m_b^2}{M_W^2}[1-(2\tau)(2I_{3f})](1+\tan^2\beta)\right)\\&-[Q_f-(2I_{3f})](2I_{3f})B^6_{\lambda,\lambda}\left(\frac{m_t^2}{M_W^2}[1+(2\tau)(2I_{3f})](1+2\cot^2\beta)+\frac{m_b^2}{M_W^2}[1-(2\tau)(2I_{3f})](1+2\tan^2\beta)\right)\\&+2Q_f^2\frac{m_f^2}{M_W^2}\{B^3_{\lambda,\lambda}[\cot^2\beta\delta_{tf}+\tan^2\beta\delta_{bf}]+B^4_{\lambda,\lambda}[(1+\cot^2\beta)\delta_{tf}+(1+\tan^2\beta)\delta_{bf}]\}\Bigg\}.\end{aligned} \tag{A20}$$

The leading terms are

$$F^{l.t.}_{\lambda,-\lambda,\tau,-\tau}\to -F^{Born}_{\lambda,-\lambda,\tau,-\tau}\left(\frac{\alpha}{32\pi s_W^2}\right)\times\left\{\left(\frac{m_t^2}{M_W^2}[3+(2\tau)](1+2\cot^2\beta)+\frac{m_b^2}{M_W^2}[1-(2\tau)](1+2\tan^2\beta)\right)\delta_{tf}+\left(\frac{m_b^2}{M_W^2}[3+(2\tau)](1+2\tan^2\beta)+\frac{m_t^2}{M_W^2}[1-(2\tau)](1+2\cot^2\beta)\right)\delta_{bf}\right\}\ln\frac{s}{M^2}, \tag{A21}$$

$$F^{l.t.}_{\lambda,\lambda,\tau,-\tau}\to 0. \tag{A22}$$

APPENDIX B: ASYMPTOTIC EXPRESSIONS OF THE BOX DIAGRAMS

The contributions of the box diagrams of Figs. 1 and 2 to the helicity amplitudes can be written in the following general form, where $i=1,\ldots,6$ correspond to the six types of box diagram. The following expressions are obtained by retaining only the logarithmic terms that appear in the complete expressions written in terms of Passarino-Veltman functions:

$$B^i_{\lambda,-\lambda}(M^2)\equiv\frac{s}{2}\sin\theta\{[\lambda+(2\tau)\cos\theta]X^i_1+s\sin^2\theta(2\tau)X^i_2\}, \tag{B1}$$

$$B^i_{\lambda,\lambda}(M^2)\equiv-\frac{s}{2}\sin\theta(2\tau)[\cos\theta X^i_1+s\sin^2\theta X^i_2+X^i_3], \tag{B2}$$

$$X^1_1=\frac{s^2+tu}{tu^2}\ln^2\frac{t}{s}+\frac{s^2+tu}{ut^2}\ln^2\frac{u}{s}-\frac{3t+2s}{ut}\ln\frac{t}{s}-\frac{3u+2s}{ut}\ln\frac{u}{s}+\frac{t-2s}{ut}\ln\frac{t}{M^2}+\frac{u-2s}{ut}\ln\frac{u}{M^2}-\frac{4s+5t+5u}{tu}\ln\frac{s}{M^2}+\frac{s}{tu}\ln^2\frac{s}{M^2}, \tag{B3}$$

$$X^1_2=\frac{s-u}{2u^3}\ln^2\frac{t}{s}-\frac{s-t}{2t^3}\ln^2\frac{u}{s}+\frac{t+3s}{2tu^2}\ln\frac{t}{s}-\frac{u+3s}{2ut^2}\ln\frac{u}{s}, \tag{B4}$$

$$X^1_3=\frac{tu-s^2}{tu^2}\ln^2\frac{t}{s}-\frac{tu-s^2}{ut^2}\ln^2\frac{u}{s}-\frac{2}{u}\ln\frac{t}{s}+\frac{2}{t}\ln\frac{u}{s}+\frac{u-t}{tu}\ln^2\frac{s}{M^2}, \tag{B5}$$

$$X^2_1=\frac{s^2+2st}{tu^2}\ln^2\frac{t}{s}+\frac{s^2+2su}{ut^2}\ln^2\frac{u}{s}-\frac{3t+4s}{2ut}\ln\frac{t}{s}-\frac{3u+4s}{2ut}\ln\frac{u}{s}-\frac{5}{2u}\ln\frac{t}{M^2}-\frac{5}{2t}\ln\frac{u}{M^2}-\frac{13s^2-4t^2-4u^2}{2stu}\ln\frac{s}{M^2}+\frac{s}{tu}\ln^2\frac{s}{M^2}-\frac{1}{t}\ln^2\frac{t}{M^2}-\frac{1}{u}\ln^2\frac{u}{M^2}, \tag{B6}$$

$$X^2_2=\frac{t-u}{2u^3}\ln^2\frac{t}{s}-\frac{u-t}{2t^3}\ln^2\frac{u}{s}+\frac{2t-3u}{2tu^2}\ln\frac{t}{s}-\frac{2u-3t}{2ut^2}\ln\frac{u}{s}, \tag{B7}$$

$$X^2_3=-\frac{s^3+4t^3+4ts^2+6st^2}{stu^2}\ln^2\frac{t}{s}+\frac{s^3+4u^3+4us^2+6su^2}{sut^2}\ln^2\frac{u}{s}+\frac{s+4t}{ut}\ln\frac{t}{s}-\frac{s+4u}{ut}\ln\frac{u}{s}+\frac{s}{ut}\ln\frac{t}{u}+\frac{2t^2+4st-2u^2-4su}{stu}\ln\frac{s}{M^2}+\left(\frac{t+2s}{2st}-\frac{u+2s}{2su}\right)\ln^2\frac{s}{M^2}+\frac{4}{s}\left(\ln^2\frac{t}{M^2}-\ln^2\frac{u}{M^2}\right), \tag{B8}$$

$$X^3_1=\frac{t}{2u^2}\ln^2\frac{t}{s}+\frac{u}{2t^2}\ln^2\frac{u}{s}+\frac{1}{u}\ln\frac{t}{s}+\frac{1}{t}\ln\frac{u}{s}, \tag{B9}$$

$$X^3_2=-\frac{t}{4u^3}\ln^2\frac{t}{s}+\frac{u}{4t^3}\ln^2\frac{u}{s}-\frac{s+3t}{4tu^2}\ln\frac{t}{s}+\frac{s+3u}{4ut^2}\ln\frac{u}{s}, \tag{B10}$$

$$X^3_3=-\frac{t}{2u^2}\ln^2\frac{t}{s}+\frac{u}{2t^2}\ln^2\frac{u}{s}-\frac{1}{u}\ln\frac{t}{s}+\frac{1}{t}\ln\frac{u}{s}, \tag{B11}$$

$$X_1^4=\frac{s}{2u^2}\ln^2\frac{t}{s}+\frac{s}{2t^2}\ln^2\frac{u}{s}-\frac{1}{u}\ln\frac{t}{s}-\frac{1}{t}\ln\frac{u}{s}, \tag{B12}$$

$$X_2^4=\frac{t-s}{4tu^2}\ln\frac{t}{s}-\frac{s}{4u^3}\ln^2\frac{t}{s}-\frac{u-s}{4ut^2}\ln\frac{u}{s}+\frac{s}{4t^3}\ln^2\frac{u}{s}, \tag{B13}$$

$$X_3^4=-\frac{s}{2u^2}\ln^2\frac{t}{s}+\frac{s}{2t^2}\ln^2\frac{u}{s}+\frac{1}{u}\ln\frac{t}{s}-\frac{1}{t}\ln\frac{u}{s}, \tag{B14}$$

$$X_1^5=\frac{2s}{tu}\ln^2\frac{t}{u}-\frac{6}{u}\ln\frac{u}{M^2}-\frac{6}{t}\ln\frac{t}{M^2}+\frac{2t+u}{tu}\ln^2\frac{t}{M^2}+\frac{2u+t}{tu}\ln^2\frac{u}{M^2}, \tag{B15}$$

$$X_2^5=\frac{3}{ut}\ln\frac{t}{u}, \tag{B16}$$

$$X_3^5=\frac{2(u-t)}{tu}\ln^2\frac{t}{u}+2\left(\frac{1}{t}\ln\frac{t}{M^2}-\frac{1}{u}\ln\frac{u}{M^2}\right)+2\left(\frac{1}{u}\ln^2\frac{t}{M^2}-\frac{1}{t}\ln^2\frac{u}{M^2}\right), \tag{B17}$$

$$X_1^6=X_3^6=0, \tag{B18}$$

$$X_2^6=\frac{1}{2tu}\ln\frac{u}{t}. \tag{B19}$$

Leading $\ln s$ and $\ln^2 s$ terms

Keeping in the above expressions only the terms proportional to $\ln(s/M^2)$ and $\ln^2(s/M^2)$, one obtains

$$B^1_{\lambda,-\lambda}=2\left(\frac{\lambda+(2\tau)\cos\theta}{\sin\theta}\right)\left(\ln^2\frac{s}{M^2}-4\ln\frac{s}{M^2}\right), \tag{B20}$$

$$B^1_{\lambda,\lambda}=8\left(\frac{(2\tau)\cos\theta}{\sin\theta}\right)\ln\frac{s}{M^2}, \tag{B21}$$

$$B^2_{\lambda,-\lambda}=\left(\frac{\lambda+(2\tau)\cos\theta}{\sin\theta}\right)\left\{4\left(\ln^2\frac{s}{M^2}-\ln\frac{s}{M^2}\right)+2\sin^2\theta\left(\frac{1}{1-\cos\theta}\ln\frac{1-\cos\theta}{2}+\frac{1}{1+\cos\theta}\ln\frac{1+\cos\theta}{2}-1\right)\right\}\ln\frac{s}{M^2}, \tag{B22}$$

$$B^2_{\lambda,\lambda}=-\frac{2(2\tau)\cos\theta}{\sin\theta}\ln^2\frac{s}{M^2}-4(2\tau)\sin\theta\ln\frac{1-\cos\theta}{1+\cos\theta}\ln\frac{s}{M^2}+2(2\tau)\cos\theta\sin\theta\left(1-\frac{1}{1-\cos\theta}\ln\frac{1-\cos\theta}{2}-\frac{1}{1+\cos\theta}\ln\frac{1+\cos\theta}{2}\right)\ln\frac{s}{M^2}, \tag{B23}$$

$$B^5_{\lambda,-\lambda}=\left(\frac{\lambda+(2\tau)\cos\theta}{\sin\theta}\right)\left\{6\left(-\ln^2\frac{s}{M^2}+2\ln\frac{s}{M^2}\right)-2\left((3-\cos\theta)\ln\frac{1-\cos\theta}{2}+(3+\cos\theta)\ln\frac{1+\cos\theta}{2}\right)\ln\frac{s}{M^2}\right\}, \tag{B24}$$

$$B^5_{\lambda,\lambda}=2\left(\frac{(2\tau)\cos\theta}{\sin\theta}\right)\left\{\ln^2\frac{s}{M^2}-4\ln\frac{s}{M^2}+\left[(3-\cos\theta)\ln\frac{1-\cos\theta}{2}+(3+\cos\theta)\ln\frac{1+\cos\theta}{2}\right]\ln\frac{s}{M^2}\right\}+4(2\tau)\sin\theta\left(\frac{1}{1+\cos\theta}\ln\frac{1-\cos\theta}{2}-\frac{1}{1-\cos\theta}\ln\frac{1+\cos\theta}{2}\right)\ln\frac{s}{M^2}. \tag{B25}$$

Using these simple expressions in Eqs. (A3),(A4),(A7),(A8),(A11), (A12),(A15),(A16),(A19),(A20), one obtains the leading terms of the helicity amplitudes given in Eqs. (A5),(A6),(A9),(A10),(A13),(A14),(A17), (A18),(A21),(A22).

APPENDIX C: THE POLARIZED $\gamma\gamma\to f\bar{f}$ CROSS SECTION

In the high energy limit, with real helicity amplitudes, the general expression of the polarized $\gamma\gamma$ cross section [19] is

$$\frac{d\sigma}{d\tau\, d\cos\theta}=\frac{d\bar{L}_{\gamma\gamma}}{d\tau}\left\{\frac{d\bar{\sigma}_0}{d\cos\theta}+\langle\xi_2\rangle\frac{d\bar{\sigma}_2}{d\cos\theta}+\langle\xi_2'\rangle\frac{d\bar{\sigma}'_2}{d\cos\theta}+\langle\xi_2\xi_2'\rangle\frac{d\bar{\sigma}_{22}}{d\cos\theta}+\langle\xi_3\rangle\cos 2\phi\frac{d\bar{\sigma}_3}{d\cos\theta}+\langle\xi_3'\rangle\cos 2\phi'\frac{d\bar{\sigma}'_3}{d\cos\theta}\right.$$

$$+\langle\xi_3\xi_3'\rangle\left[\frac{d\bar{\sigma}_{33}}{d\cos\theta}\cos 2(\phi+\phi')+\frac{d\bar{\sigma}'_{33}}{d\cos\theta^*}\cos 2(\phi-\phi')\right]+\langle\xi_2\xi_3'\rangle\cos 2\phi'\frac{d\bar{\sigma}_{23}}{d\cos\theta}-\langle\xi_3\xi_2'\rangle\cos 2\phi\frac{d\bar{\sigma}'_{23}}{d\cos\theta}\Bigg\}. \tag{C1}$$

In Eq. (C1), $\tau=s/s_{ee}$, where $s\equiv s_{\gamma\gamma}$, while $d\bar{L}_{\gamma\gamma}/d\tau$ describes the photon-photon luminosity per unit e^-e^+ flux [12]. The Stokes parameters (ξ_2,ξ_2'), (ξ_3,ξ_3'), and (ϕ,ϕ') describe, respectively, the average helicities, transverse polarizations, and azimuthal angles of the two backscattered photons. Typical values for these various quantities are given in Ref. [19]. In Eq. (C1) there appear the following quantities:

$$\frac{d\bar{\sigma}_0}{d\cos\theta}=\left(\frac{N_f}{128\pi s}\right)\sum_{\lambda_3\lambda_4}[|F_{++\lambda_3\lambda_4}|^2+|F_{--\lambda_3\lambda_4}|^2+|F_{+-\lambda_3\lambda_4}|^2+|F_{-+\lambda_3\lambda_4}|^2], \tag{C2}$$

$$\frac{d\bar{\sigma}_2}{d\cos\theta}=\left(\frac{N_f}{128\pi s}\right)\sum_{\lambda_3\lambda_4}[|F_{++\lambda_3\lambda_4}|^2-|F_{--\lambda_3\lambda_4}|^2+|F_{+-\lambda_3\lambda_4}|^2-|F_{-+\lambda_3\lambda_4}|^2], \tag{C3}$$

$$\frac{d\bar{\sigma}'_2}{d\cos\theta}=\left(\frac{N_f}{128\pi s}\right)\sum_{\lambda_3\lambda_4}[|F_{++\lambda_3\lambda_4}|^2-|F_{--\lambda_3\lambda_4}|^2-|F_{+-\lambda_3\lambda_4}|^2+|F_{-+\lambda_3\lambda_4}|^2], \tag{C4}$$

$$\frac{d\bar{\sigma}_{22}}{d\cos\theta}=\left(\frac{N_f}{128\pi s}\right)\sum_{\lambda_3\lambda_4}[|F_{++\lambda_3\lambda_4}|^2+|F_{--\lambda_3\lambda_4}|^2-|F_{+-\lambda_3\lambda_4}|^2-|F_{-+\lambda_3\lambda_4}|^2], \tag{C5}$$

$$\frac{d\bar{\sigma}_3}{d\cos\theta}=\left(\frac{-N_f}{64\pi s}\right)\sum_{\lambda_3\lambda_4}[F_{++\lambda_3\lambda_4}F_{-+\lambda_3\lambda_4}]+[F_{--\lambda_3\lambda_4}F_{+-\lambda_3\lambda_4}], \tag{C6}$$

$$\frac{d\bar{\sigma}'_3}{d\cos\theta}=\left(\frac{-N_f}{64\pi s}\right)\sum_{\lambda_3\lambda_4}[F_{++\lambda_3\lambda_4}F_{+-\lambda_3\lambda_4}]+[F_{--\lambda_3\lambda_4}F_{-+\lambda_3\lambda_4}], \tag{C7}$$

$$\frac{d\bar{\sigma}_{33}}{d\cos\theta}=\left(\frac{N_f}{64\pi s}\right)\sum_{\lambda_3\lambda_4}[F_{+-\lambda_3\lambda_4}F_{-+\lambda_3\lambda_4}], \tag{C8}$$

$$\frac{d\bar{\sigma}'_{33}}{d\cos\theta}=\left(\frac{N_f}{64\pi s}\right)\sum_{\lambda_3\lambda_4}[F_{++\lambda_3\lambda_4}F_{--\lambda_3\lambda_4}], \tag{C9}$$

$$\frac{d\bar{\sigma}_{23}}{d\cos\theta}=\left(\frac{-N_f}{64\pi s}\right)\sum_{\lambda_3\lambda_4}[F_{++\lambda_3\lambda_4}F_{+-\lambda_3\lambda_4}]-[F_{--\lambda_3\lambda_4}F_{-+\lambda_3\lambda_4}], \tag{C10}$$

$$\frac{d\bar{\sigma}'_{23}}{d\cos\theta}=\left(\frac{-N_f}{64\pi s}\right)\sum_{\lambda_3\lambda_4}[F_{++\lambda_3\lambda_4}F_{-+\lambda_3\lambda_4}]-[F_{--\lambda_3\lambda_4}F_{+-\lambda_3\lambda_4}], \tag{C11}$$

where N_f is the color factor (3 when f is a quark and 1 when it is a lepton).

Using the fact that at high energy the only nonvanishing fermion helicities are $\lambda_3=-\lambda_4\equiv\tau$, as well as the relations due to Bose symmetry and CP conservation,

$$F_{+,-,\tau,-\tau}(s,\cos\theta)=-F_{-+,\tau,-\tau}(s,-\cos\theta), \tag{C12}$$

$$F_{++,\tau,-\tau}(s,\cos\theta)=F_{--,\tau,-\tau}(s,\cos\theta)=-F_{++,\tau,-\tau}(s,-\cos\theta)=-F_{--,\tau,-\tau}(s,-\cos\theta), \tag{C13}$$

one sees that

$$\frac{d\bar{\sigma}_0}{d\cos\theta},\quad \frac{d\bar{\sigma}_3}{d\cos\theta}\equiv\frac{d\bar{\sigma}'_3}{d\cos\theta^*},\quad \frac{d\bar{\sigma}_{22}}{d\cos\theta},\quad \frac{d\bar{\sigma}_{33}}{d\cos\theta},\quad \frac{d\bar{\sigma}'_{33}}{d\cos\theta}$$

are $\cos\theta$ *symmetric*, and that

$$\frac{d\bar{\sigma}_2}{d\cos\theta}\equiv-\frac{d\bar{\sigma}'_2}{d\cos\theta},\quad \frac{d\bar{\sigma}_{23}}{d\cos\theta}\equiv-\frac{d\bar{\sigma}'_{23}}{d\cos\theta}$$

are $\cos\theta$ *antisymmetric*.

The *Born amplitudes* are such that

$$F^{Born}_{\lambda,\lambda,\tau,-\tau}(s,\cos\theta)=0, \tag{C14}$$

$$F^{Born}_{\lambda,-\lambda,\tau,-\tau}(s,\cos\theta)=-F^{Born}_{-\lambda,\lambda,-\tau,\tau}(s,\cos\theta), \tag{C15}$$

leading to the only nonvanishing Born contributions,

$$\frac{d\bar{\sigma}^{Born}_0}{d\cos\theta}\equiv-\frac{d\bar{\sigma}^{Born}_{22}}{d\cos\theta},\qquad \frac{d\bar{\sigma}^{Born}_{33}}{d\cos\theta}. \tag{C16}$$

At first order (α^3) in the electroweak corrections (i.e., neglecting the terms quadratic in $F_{\lambda,\lambda,\tau,-\tau}$), one has the additional properties

$$\frac{d\bar{\sigma}_0}{d\cos\theta} = -\frac{d\bar{\sigma}_{22}}{d\cos\theta}, \qquad \frac{d\bar{\sigma}'_{33}}{d\cos\theta} = 0, \tag{C17}$$

so that only five observables remain: the three symmetric ones

$$\frac{d\bar{\sigma}_0}{d\cos\theta} \equiv -\frac{d\bar{\sigma}_{22}}{d\cos\theta}, \qquad \frac{d\bar{\sigma}_3}{d\cos\theta} \equiv \frac{d\bar{\sigma}'_3}{d\cos\theta}, \qquad \frac{d\bar{\sigma}_{33}}{d\cos\theta},$$

and the two antisymmetric ones

$$\frac{d\bar{\sigma}_2}{d\cos\theta} \equiv -\frac{d\bar{\sigma}'_2}{d\cos\theta}, \qquad \frac{d\bar{\sigma}_{23}}{d\cos\theta} \equiv -\frac{d\bar{\sigma}'_{23}}{d\cos\theta}.$$

[1] C. Ahn *et al.*, ''Opportunities and Requirements for Experimentation at a Very High Energy e^+e^- Collider,'' Report No. SLAC-329(1928); S. Kawabata *et al.*, ''Proceedings of Workshops on Japan Linear Collider,'' KEK Reports No. 90-2, No. 91-10, No. 92-16; P.M. Zerwas, DESY Report No. 93-112, 1993; ''Proceedings of the Workshop on e^+e^- Collisions at 500 GeV: The Physics Potential,'' edited by P. Zerwas, DESY Reports No. 92-123A,B, 1992, C, 1993, D, 1994, E, 1997; E. Accomando *et al.*, Phys. Rep. **C299**, 299 (1998).

[2] R. Bossart *et al.*, ''The CLIC study of a multi-TeV e^+e^- linear collider,'' Report No. CERN-PS-99-005-LP, 1999.

[3] P. Ciafaloni and D. Comelli, Phys. Lett. B **446**, 278 (1999); M. Beccaria, P. Ciafaloni, D. Comelli, F.M. Renard, and C. Verzegnassi, Phys. Rev. D **61**, 073005 (2000); **61**, 011301 (2000); M. Beccaria, F.M. Renard, and C. Verzegnassi, *ibid.* **63**, 095010 (2001); **63**, 053013 (2001); *ibid.* (to be published), hep-ph/0103335.

[4] J.H. Kühn and A.A. Penin, hep-ph/9906545.

[5] V.V. Sudakov, Sov. Phys. JETP **3**, 65 (1956); L.D. Landau and E.M. Lifshits, *Relativistic Quantum Field Theory*, Vol. IV (MIR, Moscow, 1975).

[6] M. Kuroda, G. Moultaka, and D. Schildknecht, Nucl. Phys. **B350**, 25 (1991); G. Degrassi and A. Sirlin, Phys. Rev. D **46**, 3104 (1992); A. Denner, S. Dittmaier, and R. Schuster, Nucl. Phys. **B452**, 80 (1995); A. Denner, S. Dittmaier, and T. Hahn, Phys. Rev. D **56**, 117 (1997); W. Beenakker *et al.*, Nucl. Phys. **B410**, 245 (1993); Phys. Lett. B **317**, 622 (1993).

[7] J.H. Kühn, A.A. Penin, and V.A. Smirnov, Eur. Phys. J. C **17**, 97 (2000).

[8] P. Ciafaloni and D. Comelli, Phys. Lett. B **476**, 49 (2000); M. Ciafaloni, P. Ciafaloni, and D. Comelli, Nucl. Phys. **B589**, 359 (2000); Phys. Lett. B **501**, 216 (2001).

[9] W. Beenakker and A. Werthenbach, Phys. Lett. B **489**, 148 (2000); M. Hori, H. Kawamura, and J. Kodaira, *ibid.* **491**, 275 (2000).

[10] M. Melles, Phys. Lett. B **495**, 81 (2000); V.S. Fadin, L.N. Lipatov, A.D. Martin, and M. Melles, Phys. Rev. D **61**, 094002 (2000); M. Melles, *ibid.* **63**, 034003 (2001); hep-ph/0012196; Phys. Rev. D **64**, 014011 (2001).

[11] A. Denner and S. Pozzorini, Eur. Phys. J. C **18**, 461 (2001); hep-ph/0101213.

[12] I.F. Ginzburg, G.L. Kotkin, V.G. Serbo, and V.I. Telnov, Nucl. Instrum. Methods Phys. Res. **205**, 47 (1983); I.F. Ginzburg, G.L. Kotkin, V.G. Serbo, S.L. Panfil, and V.I. Telnov, *ibid.* **219**, 5 (1984); J.H. Kühn, E. Mirkes, and J. Steegborn, Z. Phys. C **57**, 615 (1993).

[13] V. Telnov, Int. J. Mod. Phys. A **15**, 2577 (2000); Nucl. Instrum. Methods Phys. Res. A **455**, 63 (2000); Int. J. Mod. Phys. A **13**, 2399 (1998); hep-ex/9805002; Nucl. Phys. B (Proc. Suppl.) **82**, 359 (2000); I.F. Ginzburg, *ibid.* **82**, 367 (2000); R. Brinkman, Nucl. Instrum. Methods Phys. Res. A **406**, 13 (1998); V. Telnov, talk at the International Workshop on High Energy Photon Colliders, http://www.desy.de/gg2000, 2000, DESY Hamburg, Germany; D.S. Gorbunov, V.A. Illyn, and V.I. Telnov, hep-ph/0012175.

[14] A. Denner, S. Dittmaier, and M. Strobel, Phys. Rev. D **53**, 44 (1999); A. Denner and S. Dittmaier, Eur. Phys. J. C **9**, 425 (1999).

[15] M.L. Zhou *et al.*, Phys. Rev. D **61**, 033008 (2000).

[16] M. Jacob and G.C. Wick, Ann. Phys. (N.Y.) **7**, 404 (1959).

[17] G. Passarino and M. Veltman, Nucl. Phys. **B160**, 151 (1979); K. Hagiwara, S. Matsumoto, D. Haidt, and C.S. Kim, Z. Phys. C **64**, 559 (1995).

[18] M. Beccaria, F.M. Renard, and C. Verzegnassi, hep-ph/0104245.

[19] See, e.g., G.J. Gounaris, P.I. Porfyriadis, and F.M. Renard, Eur. Phys. J. C **9**, 673 (1999), and references therein.